Title
COMPUTATION OF REACTIVE DUCT-FLOWS IN EXTERNAL FIELDS

Authors
Ben-Artzi, M.
Birman, A.

Publication Date
1988-05-01

LBL-25283
Preprint

Lawrence Berkeley Laboratory
UNIVERSITY OF CALIFORNIA

Physics Division

Mathematics Department

To be submitted for publication

Computation of Reactive Duct Flows in External Fields

M. Ben-Artzi and A. Birman

May 1988

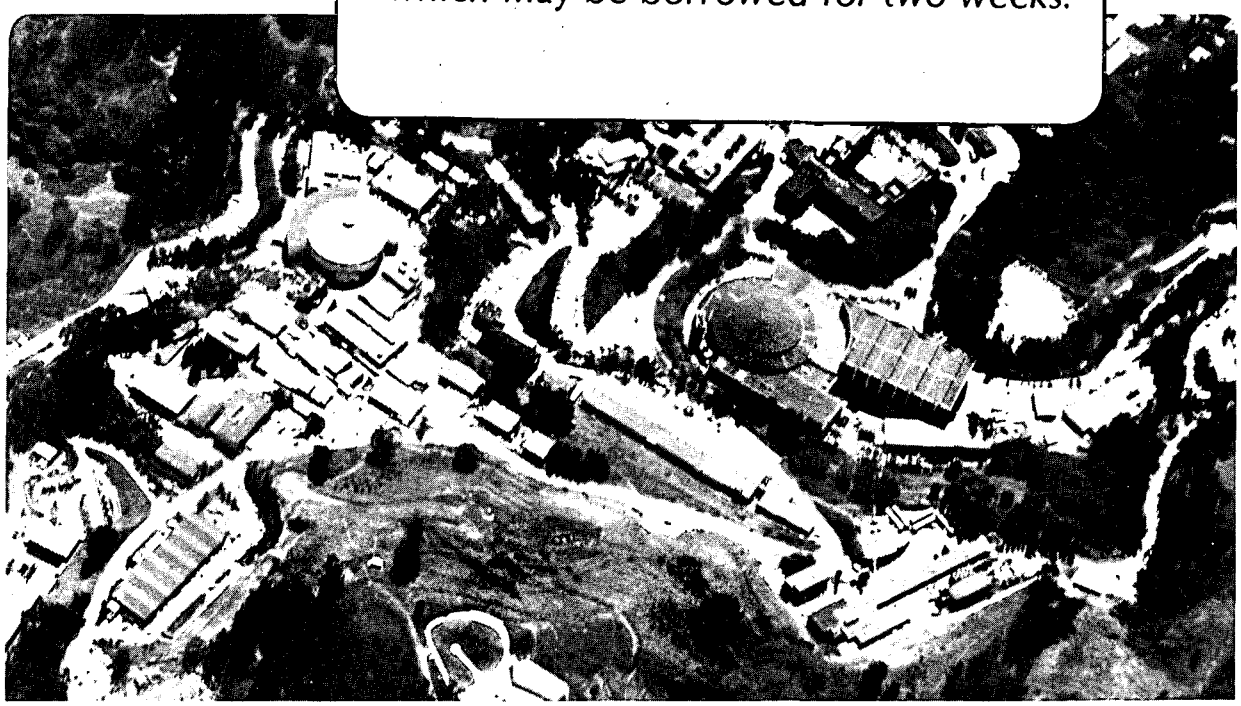

Prepared for the U.S. Department of Energy under Contract Number DE-AC03-76SF00098.

DISCLAIMER

COMPUTATION OF REACTIVE DUCT FLOWS IN EXTERNAL FIELDS[1]

Matania Ben-Artzi[2]

Department of Mathematics
Technion—Israel Institute of Technology
Haifa 32000, Israel
and
Lawrence Berkeley Laboratory
University of California
Berkeley, California 94720, USA

and

Amnon Birman

Department of Physics
Technion—Israel Institute of Technology
Haifa 32000, Israel

May 1988

[1]Also issued as Technion Preprint Series NO-MT.796.

[2]Supported in part by the Applied Mathematical Sciences Subprogram of the Office of Energy Research, U.S. Department of Energy under contract DE-AC03-76SF00098.

COMPUTATION OF REACTIVE DUCT FLOWS IN EXTERNAL FIELDS

Matania Ben-Artzi*
Department of Mathematics
Technion—Israel Institute of Technology, Haifa 32000 Israel;
and
Lawrence Berkeley Laboratory
University of California
Berkeley, CA 94720, U.S.A.

Amnon Birman
Department of Physics
Technion—Israel Institute of Technology, Haifa 32000 Israel

Abstract. A GRP-scheme is introduced for the numerical integration of the Euler system of equations of compressible reactive flow in a duct of variable cross section, subject to an external potential. The GRP (Generalized Riemann Problem) scheme is based on an analytic solution of the GRP at jump discontinuities. It is a second-order scheme generalizing the first-order Godunov scheme, having the property of high resolution of shocks and other discontinuities. Some numerical examples are considered, including an infinite spherical reflected shock, a spherical blast wave and gas collapse under an external potential.

Key Words: Reactive duct flow, Generalized Riemann Problem, External Potential, High-Resolution Scheme.

AMS Classification numbers: 35L65, 65M05, 76L05.

1. *Introduction*

Consider the Euler equations that model the time-dependent flow of an inviscid, compressible, reactive fluid through a duct of smoothly varying cross-section. In addition to the hydrodynamical pressure force, we allow an external conservative field which does not vary with time. We are using here the quasi one-dimensional approximation, namely, the hypothesis that all flow variables are uniform across a fixed cross-section. Notice that our treatment applies in particular to all problems with planar, cylindrical or spherical symmetry. Such problems arise, e.g., in astrophysics [16].

Denoting by r the spatial coordinate and by A(r) the area of the cross section at r, our equations are

$$A\frac{\partial}{\partial t}U + \frac{\partial}{\partial t}\big(AF(U)\big) + A\frac{\partial}{\partial r}G(U) + AH(U) = 0,$$

(1.1)

$$U = \begin{bmatrix}\rho\\ \rho u\\ \rho E\\ \rho z\end{bmatrix},\quad F(U) = \begin{bmatrix}\rho u\\ \rho u^2\\ (\rho E+p)u\\ \rho z u\end{bmatrix},\quad G(U) = \begin{bmatrix}0\\ p\\ 0\\ 0\end{bmatrix},\quad H(U) = \begin{bmatrix}0\\ \rho\phi'(r)\\ 0\\ k\rho\end{bmatrix},$$

where ρ,p,u are, respectively, density, pressure and velocity. z is the mass fraction of the unburnt fluid, that is, z = 1 (resp. z=0) represents the completely unburnt (resp. burnt) fluid. The total specific energy E is given by $E = e + \frac{1}{2}u^2 + \phi$, where $\phi = \phi(r)$ is the external potential (whose derivative $\phi'(r)$ is the external force field in (1.1)) and e is the specific internal energy (including chemical energy). We are assuming an equation-of-state of the form $p = p(e,\rho,z)$. The reaction rate $k = k(e,\rho,z)$ is assumed to be a positive function. Along a particle path we have $\frac{dz}{dt} = -k$, and z decreases in an irreversible way.

Our purpose in this work is to provide a robust, high-resolution numerical scheme for the time integration of the equations (1.1). We work

within the general framework of the GRP (Generalized Riemann Problem) approach [1-4], which is an analytic extension of Godunov's first-order scheme [9] and has its origins in the work of van-Leer [15]. Let us review briefly this approach, leaving the more detailed discussion to Section 7 below.

Suppose that we use equally spaced grid-points $r_i = i\cdot\Delta r$ along the r-axis and equal time-intervals of size Δt. By "cell i" we shall refer to the interval extending between the "cell-boundaries" $r_{i\pm\frac{1}{2}} = (i\pm\frac{1}{2})\Delta r$. We let Q_i^n denote the average value of a quantity Q over cell i at time $t_n = n\cdot\Delta t$. Similarly, we denote by $Q_{i+\frac{1}{2}}^{n+\frac{1}{2}}$ the value of Q at the cell-boundary $r_{i+\frac{1}{2}}$, averaged over the time interval $(n\Delta t,(n+1)\Delta t)$. Generally speaking, a "Godunov-type" difference scheme for (1.1) is given by,

$$(1.2)\qquad U_i^{n+1} - U_i^n = -\frac{\Delta t}{\Delta V_i}\left[A(r_{i+\frac{1}{2}})F(U)_{i+\frac{1}{2}}^{n+\frac{1}{2}} - A(r_{i-\frac{1}{2}})F(U)_{i-\frac{1}{2}}^{n+\frac{1}{2}}\right]$$

$$- \frac{\Delta t}{\Delta r}\left[G(U)_{i+\frac{1}{2}}^{n+\frac{1}{2}} - G(U)_{i-\frac{1}{2}}^{n+\frac{1}{2}}\right] - \Delta t\cdot H\left(U_i^{n+\frac{1}{2}}\right),$$

where $\Delta V_i = \int_{r_{i-\frac{1}{2}}}^{r_{i+\frac{1}{2}}} A(r)dr$.

While $U_i^{n+\frac{1}{2}}$ may be obtained implicitly as $\frac{1}{2}\left(U_i^n + U_i^{n+1}\right)$, one must still give an appropriate interpretation to the values $U_{i+\frac{1}{2}}^{n+\frac{1}{2}}$. In the Godunov scheme [9] this is done as follows.

Take Eq. (1.1) with $A \equiv 1$, $H \equiv 0$ and with constant initial data on both sides of $r = 0$, namely,

$$U(r,0) = \begin{cases} U_+, & r > 0 \\ U_-, & r < 0. \end{cases}$$

This constitutes the so called "Riemann Problem" (RP) and, as is well-known [8], the resulting solution $R(\frac{r}{t};\ U_+,\ U_-)$ is constant along rays $r = \lambda t$. Turning back to (1.2), consider the RP with initial conditions $U_+ = U^n_{i+1}$ and $U_- = U^n_i$. In the Godunov scheme one takes $U^{n+\frac{1}{2}}_{i+\frac{1}{2}} = R(0;\ U^n_{i+1},\ U^n_i)$, the (constant) solution along $r = 0$. As is well-known the resulting scheme is of first-order accuracy and has relatively poor resolution properties. In order to upgrade this scheme (in terms of accuracy and resolution) we assume now that the values of U are *linearly* distributed in cells, with possible jumps at $r = r_{i+\frac{1}{2}}$. To imitate the Godunov scheme, one needs to solve the resulting "initial value problem" for (1.1) at each cell-boundary. However, this is not a Riemann problem anymore, and its solutions are clearly not "self-similar". Thus, to obtain a second-order scheme we need the time evolution (to first order) of the flow variables at cell-boundaries. This leads to the formulation of the *Generalized Riemann Problem (GRP)* for (1.1) as follows:

Let $U_\pm(r)$ be two linear distributions and consider the initial value problem for (1.1) where,

$$U(r,0) = \begin{cases} U_+(r), & r > 0 \\ U_-(r), & r < 0. \end{cases} \tag{1.3}$$

Let U(r,t) be the solution. Find,

$$\text{(a)}\quad U(0,0) = \lim_{t\to 0+} U(0,t),$$

$$\text{(b)}\quad \frac{\partial U}{\partial t}(0,0) = \lim_{t\to 0+} \frac{\partial}{\partial t} U(0,t). \tag{1.4}$$

Note that the application of the GRP to the numerical scheme (1.2) is straightforward. Indeed, one takes in (1.3) the two linear distributions as given by the values of U^n is cells i and i+1, translating $r_{i+\frac{1}{2}}$ to 0.

Taking $t_n = 0$, the solution (1.4) is obtained and then interpreted as,

$$U^n_{i+\frac{1}{2}} = U(0,0), \qquad \left[\frac{\partial}{\partial t}U\right]^n_{i+\frac{1}{2}} = \frac{\partial U}{\partial t}(0,0).$$

Finally, one sets in (1.2),

$$U^{n+\frac{1}{2}}_{i+\frac{1}{2}} = U^n_{i+\frac{1}{2}} + \frac{\Delta t}{2}\left[\frac{\partial}{\partial t}U\right]^n_{i+\frac{1}{2}}. \tag{1.5}$$

The existence of a solution to the GRP has been studied in detail in several recent works [10,12]. Its wave pattern in a small neighborhood of the singularity is completely determined by the solution $R(\frac{r}{t};U_+,U_-)$ to the *Associated Riemann Problem*, which is the RP with initial conditions equal to the limiting values of the linear initial data at the discontinuity, that is, using (1.3),

$$U_+ = U_+(0+) = \lim_{r\to 0+} U_+(r), \qquad U_- = U_-(0-) = \lim_{r\to 0-} U_-(r). \tag{1.6}$$

We have the following.

Proposition. *Let $U(r,t)$ be the solution to the GRP (1.1),(1.3) and let $R(\frac{r}{t};U_+,U_-)$ be the solution of the associated RP. Then for every fixed direction $\lambda = \frac{r}{t}$,*

$$\lim_{t\to 0+} U(\lambda t,t) = R(\lambda;U_+,U_-). \tag{1.7}$$

Furthermore, the wave configuration for the GRP near the singularity is the same as that for the associated RP.

The last part of the proposition means that if the solution $R(\frac{r}{t};U_+,U_-)$ involves a shock moving to the right, then this is the case also for the GRP (even though its trajectory is not a straight line anymore), etc.

Our work is an extension of [4], where planar combustion waves were considered. Many of the results here are parallel to those obtained in the planar case, with suitable modifications due to the presence of external fields and a variable cross section. Whenever this is the case, we state clearly the result and list the modified formulae, but omit the proof, giving suitable reference to [4].

The plan of the paper is as follows. In Section 2 we set up our notation (for convenience we display it in Table I) and discuss the basic thermodynamical and characteristic relations of the system. We also introduce the Lagrangian version of the equations. In Section 3 we give a detailed analysis of a centered rarefaction wave, which is really the heart of the GRP method. In Sections 4 and 5 we give the solution to the GRP in the Lagrangian and Eulerian frames, respectively. In Section 6 we specialize our results to a γ-law gas (where γ is independent of the chemical structure) with a simplified Arrhenius model for the chemistry. This leads to explicit (closed form) formulae for the solution of the GRP, due to the fact that the associated RP is explicitly solvable in this case.

Section 7 carries the reward for our labor in the preceding sections. We use a straightforward GRP scheme along the lines discussed above, namely, combining (1.2) and (1.5) (a few more details concerning the numerical scheme are added in that section). Three numerical examples are discussed in Section 7: (a) A test problem suggested by W.F. Noh [13] which involves a single reflected infinite shock in spherical geometry; (b) A spherical explosion originating at the center of a uniform gas in spherical geometry [14]; (c) the collapse of a gas cluster under an

external field (simulating self-gravity), with and without chemical reactions [16]. We observe that example (a) has no chemistry or external potentials and has a full analytic solution. Example (b) possesses an analytic solution in the limit of infinite reaction rate (C-J theory) and contains chemistry but no external potentials. Example (c) contains all the novel features of the scheme presented here.

The only previous (numerical) treatment of the system (1.1), that we are aware of, is given in [16]. However, the method presented there does not seem to have the same order of accuracy in the time integration. A comparison of the results in [16] with the results obtained here is given in Section 7.

Acknowledgements

Part of this work was written while M. Ben-Artzi was visiting the Department of Mathematics at the Lawrence Berkeley Laboratory, University of California, during the Summer of 1987. It is a pleasure to acknowledge the warm hospitality of the department and, in particular, Professors A. Chorin and P. Concus.

A. Birman would like to thank Professor A. Yahil for useful discussions.

2. *Preliminaries and Notation*

In what follows we shall address the GRP as stated in (1.3),(1.4). In addition to the basic flow variables appearing in (1.1), we shall also make extensive use of the speed of sound c and the "Lagrangian" speed of sound $g = \rho c$. Recall that c^2 is obtained by differentiating p with respect to ρ along an isentropic curve. However, the concept of entropy needs to be clarified here. Thus, let $T = T(e,\rho,z)$ be the temperature. For each *fixed* z we define the entropy $S(e,\rho,z)$ as usual by,

$$TdS_z \equiv T\left(\frac{\partial S}{\partial e}de + \frac{\partial S}{\partial \rho}d\rho\right) = de + pd\left(\frac{1}{\rho}\right). \tag{2.1}$$

Solving for e we get $e = e(\rho,S,z)$ and substituting this in the equation-of-state we get $p = p(S,\rho,z)$. We then set,

$$c^2 = \frac{\partial p}{\partial \rho}(S,\rho,z). \tag{2.2}$$

We shall always indicate the independent variables when differentiating a thermodynamical function, as has been done in (2.2). Another important function in our analysis will be,

$$\lambda(e,\rho,z) = k(e,\rho,z)\frac{\partial}{\partial z}p(e,\rho,z), \tag{2.3}$$

where the reaction rate k is as in (1.1).

It can easily be checked that the first three equations of (1.1) yield the characteristic relation,

$$\frac{de}{dt} + p\frac{d}{dt}\left(\frac{1}{\rho}\right) = 0 \quad \text{along } \frac{dr}{dt} = u. \tag{2.4}$$

Using (2.1) and the fourth equation in (1.1) this can be written as,

$$(2.5)\quad \frac{dS}{dt} = \frac{\partial}{\partial z}S(e,\rho,z) \cdot \frac{dz}{dt} = -\,k(e,\rho,z)\frac{\partial}{\partial z}S(e,\rho,z) \equiv -\,f \text{ along } \frac{dr}{dt} = u.$$

We now transform the system (1.1), replacing the coordinate r by the Lagrangian coordinate ξ given by,

$$(2.6)\qquad d\xi = A\rho dr, \qquad \xi(0) = 0.$$

Replacing the third equation of (1.1) by (2.5), the system can now be written as,

$$(2.7)\qquad V_t + \Phi(V)_\xi = \Psi(V),$$

$$V = \begin{bmatrix}\tau\\ u\\ S\\ z\end{bmatrix},\quad \Phi(V) = A\cdot\begin{bmatrix}-u\\ p\\ 0\\ 0\end{bmatrix},\quad \Psi(V) = \begin{bmatrix}0\\ n\cdot\frac{p}{\rho}-\phi'\\ -f\\ -k\end{bmatrix},\quad \tau = \frac{1}{\rho},\ n(r) = \frac{A'(r)}{A(r)}.$$

Observe that in (2.7) the functions $n(r),\phi(r)$ depend on ξ,t by expressing $r = r(\xi,t)$ in the Lagrangian frame.

The Characteristic Relations. Obviously the contact discontinuity (= particle path) ξ = const. serves as a double "linearly degenerate" characteristic, with the last two equations in (2.7) as its associated characteristic relations. It is not difficult to see that the other two characteristic directions are given by $\frac{d\xi}{dt} = \pm\, gA$ (recall that $g = \rho c$). Proceeding along the same line as in [4. Sec.2] we obtain the following characteristic relations,

$$(2.8))\qquad gdu \pm dp = \left[\,\mp\,\lambda\,\mp\, gucn - g\phi'\right]dt, \text{ along } \frac{d\xi}{dt} = \pm\, gA,$$

where n,λ are the functions defined in (2.7),(2.3), respectively.

Note that the right-hand side in (2.8) consists of three contributions asociated, respectively, with the chemistry equation, variable cross section and external potential. They all vanish for planar non-reactive flow without external fields, where $\Psi \equiv 0$ in (2.7). Their magnitudes determine the amount by which the system (2.7) deviates from the corresponding one with $\Psi \equiv 0$. In particular, the magnitude of λ reflects the coupling between the compressible flow and the chemistry equation in (2.7).

Finally, we introduce some notation for the treatment of the GRP for the system (2.7). We assume that initially $V(\xi,0) = V_{\pm}(\xi)$ is piecewise linear with a jump at $\xi = 0$, in analogy to (1.3). This is justified by the fact (to be proved below) that the time derivatives at the singularity depend only on the *limiting* values (as $\xi \to 0$) of the initial data (including slopes). Hence we may replace r-derivatives by ξ-derivatives according to (2.6). Letting $V_- = \lim_{\xi\to 0-} V_-(\xi)$, $V_+ = \lim_{\xi\to 0+} V_+(\xi)$ (compare with (1.6)), we denote by $R_L\left(\frac{\xi}{t};V_+,V_-\right)$ the Lagrangian solution to the associated Riemann problem (see the Proposition and the discussion preceding it in the Introduction). Denoting by $V(\xi,t)$ the solution to the GRP for (2.7), our objective (in analogy with (1.4)) is to determine,

$$V(0,0) = \lim_{t\to 0+} V(0,t),$$

$$\frac{\partial V}{\partial t}(0,0) = \lim_{t\to 0+} \frac{\partial}{\partial t} V(0,t).$$

Clearly, in this case the line $\xi = 0$ represents a contact discontinuity across which ρ,S,z may be discontinuous, so that we must compute the corresponding limiting values on both sides of this line.

We shall employ the following notation conventions: Subscripts "$_+,_-$" denote limiting values as $\xi \to 0+, 0-$, respectively; an asterisk (*) is used for values at t=0+ along $\xi=0$ (along with "$_+,_-$" for discontinuous quantities). Further details are given in Table I, where $Q = Q(\xi,t)$ stands for any one of the flow variables (see also Figure 1 in Section 3 below).

Table I — Notations for the Lagrangian GRP

Symbol	Definition
Q_+, Q_-	$\lim Q(\xi,0)$ as $\xi \to 0+, 0-$
$(\frac{\partial Q}{\partial \xi})_+, (\frac{\partial Q}{\partial \xi})_-$	Constant (initial) slopes for $\xi>0$, $\xi<0$
$R_L(\frac{\xi}{t}; V_+, V_-)$	Lagrangian solution of the associated RP
V^*	$= R_L(0; V_+, V_-)$
Q_+^*, Q_-^*	Right and left values for Q discontinuous across $\xi=0$ (e.g., $Q = \rho$ or g)
$(\frac{\partial Q}{\partial t})^*$	$\lim_{t\to 0+} \frac{\partial}{\partial t} Q(\xi,t)$ at $\xi=0$
$(\frac{\partial Q}{\partial t})_+^*, (\frac{\partial Q}{\partial t})_-^*$	Right and left values of $(\frac{\partial Q}{\partial t})^*$ for discontinuous Q
$(\frac{\partial Q}{\partial \xi})_+^*$	$= \lim_{t\to 0+} \lim_{\xi\to 0+} \frac{\partial}{\partial \xi} Q(\xi,t)$
$(\frac{\partial Q}{\partial \xi})_-^*$	$= \lim_{t\to 0+} \lim_{\xi\to 0-} \frac{\partial}{\partial \xi} Q(\xi,t)$
$(\frac{\partial Q}{\partial t})_+, (\frac{\partial Q}{\partial t})_-$	$= \lim_{\xi\to 0+} \frac{\partial}{\partial t} Q(\xi,t)\Big\|_{t=0}, \lim_{\xi\to 0-} \frac{\partial}{\partial t} Q(\xi,t)\Big\|_{t=0}$

Remark. Note that if two limiting processes are implied, they must be carried out in the indicated order. For example $(\frac{\partial Q}{\partial \xi})^*_+$ means that first the ξ-derivative is evaluated at ξ=0+ and its limit is then taken as t→0+. Thus, the evaluation of $(\frac{\partial Q}{\partial \xi})^*_+$ depends on the full solution of the GRP. On the other hand, $(\frac{\partial Q}{\partial t})_+$ is computed by first taking the t-drivative at t=0 (which requires only the initial data and the system (2.7)) and then letting ξ→0+. So, we can form the following groups of variables and their derivatives:

$Q_\pm, (\frac{\partial Q}{\partial \xi})_\pm$, are the given initial data;

$(\frac{\partial Q}{\partial t})_\pm$ are evaluated from (2.7) and the initial data;

$Q^*, Q^*_\pm$ are derived from the associated RP;

$(\frac{\partial Q}{\partial t})^*, (\frac{\partial Q}{\partial \xi})^*_\pm$ are derived from the solution to the GRP.

3. *Resolution of a Centered Rarefaction Wave (CRW)*

The jump discontinuity of the initial data is resolved in terms of a shock, contact discontinuities and centered rarefaction waves. The main analytical ingredient in the GRP scheme is a detailed resolution of the CRW. We refer the reader to Section 3 of [4] for a full discussion of this issue. The basic idea is to use characteristic coordinates (α,β) throughout the CRW, so that the singularity is "blown-up" into a "full segment" $\alpha=0$ in the characteristic plane.

Consider Figure 1, where a CRW travelling to the left is shown. We let $\Gamma^+:\alpha$ = const. be the family of chracteristic curves associated with the slope $+gA$ (see (2.8)) and $\Gamma^-:\beta$ = const. the family associated with the slope $-gA$. In accordance with the Proposition stated in the Introduction, the values of flow variables along Γ^--curves converge (as the singularity is approached) to the corresponding values for the associated RP. In particular, we can take the coordinate β as the normalized slope of Γ^- at $\xi=0$, so that

$$\beta = \begin{cases} 1 & \text{at the head characteristic,} \\ \beta^* = \dfrac{g_-^*}{g_-} & \text{at the tail characteristic .} \end{cases} \tag{3.1}$$

Figure 1

The characteristic coordinate α, for a given Γ^+ curve, is taken as the ξ-coordinate of its intersection with the head characteristic ($\beta=1$) of the Γ^- rarefaction fan. Thus $\alpha=0$ is the singularity.

All variables, including ξ,t, are taken as functions of α,β. In particular, the connection between the solution $V(\alpha,\beta)$ to the GRP, and its associated RP, can be expressed as,

(3.2) $\quad V(0,\beta) = R_L(-g_A(0)\beta;V_+,V_-)$ (see Table I of Section 2).

(Of course we can normalize here, $A(0) = 1$). From the last two equations in (2.7) we see that S,z, are allowed to jump only across a contact discontinuity ($\xi=0$), so that (3.2) implies,

(3.3) $\quad S(0,\beta) \equiv S_, \qquad z(0,\beta) \equiv z_.$

As for the transformation $(\alpha,\beta) \to (\xi,t)$, one can prove, in a way which is completely analogous to the proof of Proposition 3.1 in [4] that,

$$
\begin{aligned}
\xi(\alpha,\beta) &= \alpha\beta^{\frac{1}{2}} + \epsilon(\alpha,\beta) \cdot \alpha^2, \\
t(\alpha,\beta) &= -g_^{-1}A(0)^{-1}\beta^{-\frac{1}{2}}\alpha + \eta(\alpha,\beta) \cdot \alpha^2.
\end{aligned}
\tag{3.4}
$$

Next, we note that even though the limiting values $S(0,\beta)$, $z(0,\beta)$ are constant (see (3.3)), the limiting values of the gradients (along Γ^- characteristics) $S_\alpha(0,\beta)$, $z_\alpha(0,\beta)$ do not necessarily vanish and, in fact, depend on β. This is due to the presence of source terms in the equations (2.7) for S,z. The following proposition describes the way in which these gradients vary with β. Observe that the variable cross section does not play any role here while the initial slopes enter the equations only through the initial conditions (3.6). The proof of the proposition follows verbatim that of Proposition 3.2 in [4] and will be omitted.

Proposition 3.1. *Let f,k in the system (2.7) be expressed in terms of the variables p,S,z. Then the functions* $S_\alpha(0,\beta)$, $z_\alpha(0,\beta)$ *satisfy (as functions of* β, $\beta^* \leq \beta \leq 1$*) the following relations,*

$$\text{(i)}\quad \frac{d}{d\beta}\left(\beta^{-\frac{1}{2}} S_\alpha(0,\beta)\right) = -g_-^{-1}A(0)^{-1}\beta^{-2} f\left(p(0,\beta),S_-,z_-\right),$$

(3.5)

$$\text{(ii)}\quad \frac{d}{d\beta}\left(\beta^{-\frac{1}{2}} z_\alpha(0,\beta)\right) = -g_-^{-1}A(0)^{-1}\beta^{-2} k\left(p(0,\beta),S_-,z_-\right),$$

supplemented with the initial conditions (at $\beta=1$*),*

$$\text{(i)}\quad S_\alpha(0,1) = \left(\frac{\partial S}{\partial \xi}\right)_- + g_-^{-1} f(p_-,S_-,z_-),$$

(3.6)

$$\text{(ii)}\quad z_\alpha(0,1) = \left(\frac{\partial z}{\partial \xi}\right)_- + g_-^{-1} k\left(p_-,S_-,z_-\right).$$

Having at our disposal the functions $S_\alpha(0,\beta)$, $z_\alpha(0,\beta)$, we can now proceed to derive expressions for the gradients $Q_\alpha(0,\beta)$ of all flow variables. This is indeed the heart of the GRP method [1,2,3,4]. As in previous applications of this method, it turns out that it is easiest to start out with an expression for $u_\alpha(0,\beta)$. In what follows we use the functions λ,n as in (2.3),(2.7), respectively. We have,

Theorem 3.2. *Let* $a(\beta) = \frac{\partial}{\partial \alpha} u(\alpha,\beta)\big|_{\alpha=0}$, *and let* $g = \rho c$ *be represented as* $g(p,S,z)$. *Then* $a(\beta)$ *satisfies,*

$$\frac{d}{d\beta} a(\beta) = Y(\beta), \qquad \beta^* \leq \beta \leq 1, \tag{3.7}$$

where,

$$\begin{aligned} Y(\beta) = {} & -\tfrac{1}{2} g_-^{-1} A(0)^{-1} \beta^{-\frac{1}{2}} \frac{d}{d\beta}\left(\beta^{-1}\lambda(0,\beta)\right) \\ & - \tfrac{1}{2} g_-^{-1}\beta^{-1}\cdot\left[g_S(0,\beta)\cdot S_\alpha(0,\beta) + g_z(0,\beta)\cdot z_\alpha(0,\beta)\right]\cdot \frac{d}{d\beta} u(0,\beta) \\ & - \tfrac{1}{2} g_-^{-1} A(0)^{-1} n(0)\cdot\beta^{-\frac{1}{2}}\cdot\frac{d}{d\beta}\left(u(0,\beta)\cdot c(0,\beta)\right) - \tfrac{1}{2} g_-^{-1} A(0)^{-1}\phi'(0)\beta^{-\frac{3}{2}}. \end{aligned} \tag{3.8}$$

This equation is supplemented by the initial condition,

$$a(1) = \left(\frac{\partial u}{\partial \xi}\right)_- + g_-^{-1}\left(\frac{\partial p}{\partial \xi}\right)_- + A(0)^{-1}g_-^{-1}\phi'(0). \tag{3.9}$$

The proof of the theorem proceeds along the same lines as that of Theorem 3.3 in [4] and will be omitted. We note that $Y(\beta)$ is the sum of four terms which are related to different effects in the system (2.7) (or (1.1)). Thus the first one is a contribution of the chemical source term, the second originates from the non-zero slopes of initial data, the third is due to the variation of cross section and the fourth comes from the presence of a non-constant external potential.

Once the theorem is established, it is easy to derive expressions for the characteristic slopes of other flow variables. They are obtained from the characteristic relations (2.8) and the representation of ρ in terms of p,S,z (where we have (2.2)).

Corollary 3.3. *The characteristic slopes of p,ρ in the rarefaction fan are given by,*

$$\begin{aligned}\frac{\partial p}{\partial \alpha}(0,\beta) &= g_-\cdot\beta a(\beta) + g_-^{-1}A(0)^{-1}\beta^{-\frac{1}{2}} \\ &\quad\cdot\left[\lambda(0,\beta) + g_-\cdot\beta u(0,\beta)c(0,\beta)\cdot n(0) - g_-\cdot\beta\phi'(0)\right], \\ \frac{\partial \rho}{\partial \alpha}(0,\beta) &= c(0,\beta)^{-2}\,\frac{\partial p}{\partial \alpha}(0,\beta) + \frac{\partial \rho}{\partial S}(p(0,\beta),S_-,z_-)\cdot\frac{\partial S}{\partial \alpha}(0,\beta) \\ &\quad + \frac{\partial \rho}{\partial z}(p(0,\beta),S_-,z_-)\cdot\frac{\partial z}{\partial \alpha}(0,\beta).\end{aligned} \tag{3.10}$$

4. *The Lagrangian Solution of the GRP*

In this section we give the full solution of the generalized Riemann problem (1.3)-(1.4) in the Lagrangian setting (2.7). We seek here expressions for $(\frac{\partial V}{\partial t})^*$ (see Table I in Section 2) in terms of the initial data, having a jump discontinuity at $\xi=0$. Velocity and pressure are continuous across the interface, and since the time derivatives of S,z are given by the system (2.7) directly (different on the two sides of $\xi=0$!) it remains only to evaluate $(\frac{\partial p}{\partial t})^*, (\frac{\partial u}{\partial t})^*$. An essential feature of the GRP method is that these two derivatives can be easily determined from the initial data and the solution V* of the associated RP. In fact, we have,

Theorem 4.1. *Assume the configuration of Figure 1 (Section 3). The derivatives* $(\frac{\partial p}{\partial t})^*$, $(\frac{\partial u}{\partial t})^*$ *satisfy a pair of linear equations,*

$$a_-(\frac{\partial u}{\partial t})^* + b_-(\frac{\partial p}{\partial t})^* = d_- \ , \tag{4.1}$$

$$a_+(\frac{\partial u}{\partial t})^* + b_+(\frac{\partial p}{\partial t})^* = d_+ \ . \tag{4.2}$$

The coefficients a_+, b_+, d_+ *(resp.* a_-, b_-, c_-*) are determined explicitly from the values of the RP solution* V* *and the initial conditions* $V_+, (\frac{\partial V}{\partial \xi})_+$ *(resp.* $V_-, (\frac{\partial V}{\partial \xi})_-$*). More specifically, on the rarefaction side we have,*

$$\begin{aligned} a_- &= 1 \ , \qquad b_- = (g_-^*)^{-1} \ , \\ d_- &= -A(0)\cdot(g_-g_-^*)^{\frac{1}{2}}\cdot a(\beta^*) - u^*c_-^*\cdot n(0) - (g_-^*)^{-1}\cdot\lambda(0,\beta^*), \end{aligned} \tag{4.3}$$

where $a(\beta)$ *is as in Theorem 3.2 and the functions* λ, n, *are defined by* (2.3), (2.7).

For a_+, b_+, d_+ one uses the Hugoniot (u,p) relation. Explicit expressions for a γ-law gas are given in Theorem 6.3 below.

The proof of this theorem is again parallel to that of Theorem 4.1 in [4] and will be omitted. Observe that while the variation of the cross section, n(0), appears in the expression for d_-, the potential ϕ does not play a role here.

Once the time derivatives of p,u along $\xi=0$ (a streamline) are determined, it is easy to compute the full array of such derivatives, namely $\left(\frac{\partial V}{\partial t}\right)^*$. Furthermore, using once again the notation of Table I, Section 2, the spatial derivatives $\left(\frac{\partial V}{\partial \xi}\right)^*_{\pm}$ at the contact discontinuity can be evaluated with the help of the basic equations (2.7). We refer the reader to the Appendix below for the detailed expressions. However, the following observation is important.

Proposition 4.2. *In Lagrangian coordinates, along any line ξ = const., one has,*

$$\frac{\partial \rho}{\partial t} = c^{-2}\left[\frac{\partial p}{\partial t} + \lambda(e,\rho,z)\right]. \tag{4.4}$$

Proof. Write ρ in terms of p,S,z, so that along a particle path, by (2.2),(2.5),

$$\frac{\partial \rho}{\partial t} = c^{-2}\frac{\partial p}{\partial t} + \rho_S \frac{\partial S}{\partial t} + \rho_z \frac{\partial z}{\partial t} = c^{-2}\frac{\partial p}{\partial t} - k\left[\rho_S \frac{\partial S(e,\rho,z)}{\partial z} + \rho_z\right].$$

But using the identity $\rho = \rho\big(p(e,\rho,z), S(e,\rho,z), z\big)$ we get by differentiation,

$$\rho_S \frac{\partial S(e,\rho,z)}{\partial z} + \rho_z = -\rho_p \frac{\partial p(e,\rho,z)}{\partial z},$$

which implies (4.4) (see (2.3) for the definition of λ).

□

It is interesting to compare (4.4) with its "non-reactive" analogue $\frac{\partial \rho}{\partial t} = c^{-2} \frac{\partial p}{\partial t}$. Thus, the deviation along a streamline is proportional to λ. This is in line with the characteristic expressions (2.8), where the magnitude of λ reflects the strength of the coupling between the fluid-dynamical (compressible) phase of the flow and the chemical (reactive) phase.

5. *The Eulerian Solution of the GRP*

In this section we address the main goal of this work, namely, the solution of the GRP (1.3)-(1.4) for the system (1.1).

Once again we assume the wave configuration of Figure 1, with the jump located at r=0. As an auxiliary tool we shall use the Lagrangian coordinate ξ, defined by (2.6). As was shown in the previous discussion, the time derivatives at the singularity depend only on the spatial slopes as $\xi \to 0$. We may therefore assume that the initial values of flow variables are simultaneously linear in r and ξ (on either side of the jump), with slopes related by,

$$(5.1) \qquad \left(\frac{\partial Q}{\partial \xi}\right)_{\pm} = A(0)^{-1}\rho_{\pm}^{-1}\left(\frac{\partial Q}{\partial r}\right)_{\pm}.$$

Using the notation in (1.4) we see by (1.7) that,

$$(5.2) \qquad U(0,0) = R(0;U_+,U_-).$$

In order to evaluate $\frac{\partial U}{\partial t}(0,0)$ we shall simply use the chain rule and the derivatives along $\xi=0$. To this end let $\xi(t)$ denote the representation of r=0 in the (ξ,t) frame. Clearly, $r(\xi(t),t) \equiv 0$ and (2.6) imply,

$$(5.3) \qquad \xi'(t) = -A(0)\rho(\xi(t),t)\cdot u(\xi(t),t), \quad \xi(0) = 0.$$

Thus, if Q is any flow variable which can be expressed either in the Eulerian or Lagrangian coordinates (displaying coordinates for clarity), we obtain

$$\left.\frac{\partial Q(r,t)}{\partial t}\right|_{r=0} = \left.\frac{\partial Q(\xi,t)}{\partial t}\right|_{\xi=\xi(t)} - A(0)\rho(0,t)u(0,t)\cdot\left.\frac{\partial Q(\xi,t)}{\partial \xi}\right|_{\xi=\xi(t)}.$$

Observe that when $t\to 0$, the left-hand side in this equation converges to the GRP solution $\frac{\partial Q}{\partial t}(0,0)$ while in the right-hand side we get limits which are all known from the Lagrangian solution. Indeed, by (1.7) we have,

$$\rho(0,t)u(0,t) \to \rho(0,0)u(0,0),$$

which is the associated RP solution along $r=0$. Also, the limits of the derivatives $\frac{\partial Q(\xi,t)}{\partial t}$ and $\frac{\partial Q(\xi,t)}{\partial \xi}$ are determined by the position of $\xi(t)$ relative to the various waves. For example, if $\xi(t)$ lies between the contact discontinuity ($\xi=0$) and the shock moving to the right, then by the notation of Table I, Section 2,

$$\frac{\partial Q(\xi,t)}{\partial t}\Big|_{\xi=\xi(t)} \to \left(\frac{\partial Q}{\partial t}\right)^*_+, \qquad \frac{\partial Q(\xi,t)}{\partial \xi}\Big|_{\xi=\xi(t)} \to \left(\frac{\partial Q}{\partial \xi}\right)^*_+, \quad \text{as } t\to 0.$$

Of course, these considerations are only valid if $r=0$ is not contained in a rarefaction fan, namely, that it is not a sonic line.

To summarize the above, we have,

Theorem 5.1. *(Non-Sonic Case).. In the non-sonic case the Eulerian solution to the GRP is given by*

$$\frac{\partial U}{\partial t}(0,0) = \lim_{t\to 0}\left[\frac{\partial U(\xi,t)}{\partial t}\Big|_{\xi=\xi(t)} - A(0)\rho(0,0)u(0,0)\cdot\frac{\partial U(\xi,t)}{\partial \xi}\Big|_{\xi=\xi(t)}\right]. \tag{5.4}$$

The derivatives in the right-hand side are determined from the Lagrangian solution to the GRP and the position of $\xi=\xi(t)$ (i.e., $r=0$) in the wave configuration.

We remark that by the discussion following the Proposition in the Introduction, the position of $\xi(t)$ is also determined by the solution to the associated RP.

Finally, let us turn to the *Sonic Case*. Here, of course, (5.4) is meaningless and we have to go back to the characteristic structure of the fan as discussed in Section 3. Throughout the fan, a variable Q is expressed as $Q(\alpha,\beta)$. The line r=0 is sonic, so that it is tangent to some Γ^--curve (Figure 1) $\beta=\beta_0$. The slope β_0 is determined by,

$$u(0,\beta_0) = c(0,\beta_0), \tag{5.5}$$

where $u(0,\beta)$, $c(0,\beta)$ are as in (3.2).

Now r=0 is represented in the fan by $(\alpha(t),\beta(t))$ (replacing $\xi(t)$ of (5.3)) and instead of (5.4) one obtains,

$$\frac{\partial U}{\partial t}(0,0) = \frac{\partial U}{\partial \alpha}(0,\beta_0)\cdot\alpha'(0) + \frac{\partial U}{\partial \beta}(0,\beta_0)\cdot\beta'(0). \tag{5.6}$$

The right-hand side in (5.6) is known from the solution (Section 3) of the CRW. More specifically, we have,

Theorem 5.2. *(Sonic Case). Let r=0 be a sonic line represented by* $(\alpha(t),\beta(t))$ *with* $(\alpha(0),\beta(0)) = (0,\beta_0)$ *in the* Γ^-*-rarefaction fan. Let* $U(\alpha,\beta)$ *be the solution of the GRP in the fan, where* $U(0,\beta)$ *is (by (1.7)) the solution for the associated RP and the variation* $\frac{\partial}{\partial\alpha}U(\alpha,\beta)\big|_{\alpha=0}$ *is obtained in Section 3 (Theorem 3.2 and Corollary 3.3). Then the solution of the GRP in Eulerian coordinates is given by Equation (5.6) where,*

$$\begin{aligned} \alpha'(0) &= -A(0)g_-\cdot\beta_0^{\frac{1}{2}}, \\ \beta'(0) &= \frac{1}{2}A(0)\beta_0^{\frac{1}{2}}\left[\frac{\partial g}{\partial\alpha}(0,\beta_0) - \frac{\partial}{\partial\alpha}(\rho u)(0,\beta_0)\right]. \end{aligned} \tag{5.7}$$

The proof of the formulae (5.7) is identical with that given in Section 5 of [4] and will be omitted.

6. *A Special Case: γ-Law Gas and a Simplified Arrhenius Model*

In this section we give explicit formulae for the case in which the equation of state is given by

$$p = (\gamma-1)\rho(e-q_0 z),\ \gamma > 1,\ q_0 > 0, \tag{6.1}$$

where q_0 is the constant chemical energy released when a unit mass of unburnt gas is totally burnt and the adiabatic exponent γ is fixed independently of the other thermodynamic variables.

From our definition of entropy (2.1), combined with (6.1), we see that a suitable choice for S could be,

$$S = \frac{1}{\gamma-1}\frac{p}{\rho^\gamma} = \rho^{1-\gamma}(e-q_0 z). \tag{6.2}$$

In addition to equation (6.1) we take a reaction rate (the function k of (1.1)) which is a "simplified Arrhenius" model, as in [4,7],

$$k = K\cdot z\cdot H(T-T_C),\quad K > 0,\quad T = \frac{p}{\rho}, \tag{6.3}$$

where,

$$H(x) = \begin{cases} 1, & x > 0, \\ 0, & x \leqslant 0, \end{cases}$$

and T_C is a given ("critical") temperature. The variation of entropy along a streamline (see equation (2.5)) is then given by,

$$f = -Kq_0\rho^{1-\gamma}z\cdot H(T-T_C), \tag{6.4}$$

and the function λ (see Equation (2.3)) which represents the contribution of the chemistry to the variation of the Riemann invariants (see Equation (2.8)) is given by,

$$\lambda(\rho,p,z) = -(\gamma-1)Kq_0\rho z\cdot H(T-T_C). \tag{6.5}$$

Observe that the magnitude of λ is essentially determined by the product Kq_0, which therefore reflects the amount of "coupling" between the chemical and the fluid dynamical phases of the flow (compare with the remarks following Equation (2.8)).

In the case at hand, the solution of the GRP can be obtained explicitly. This means that one has explicit expressions for the characteristic derivatives in the CRW (Section 3), and in particular for $a(\beta)$ (Theorem 3.2). Also, the Hugoniot curve in this case is given by an explicit algebraic expression. Hence one can calculate (in closed form) the coefficients $a_{\pm}$, $b_{\pm}$ and $d_{\pm}$ in Theorem 4.1, as well as β_0 and the other quantities needed in the sonic case (Theorem 5.2).

Clearly, the solution to the associated RP in our case is identical with that of [4], so we skip it completely. The reader may find the details in Proposition 6.1 there. Also, all the expressions in the simplified model here are obtained by straightforward substitution in the general formulae of Sections 3,4 above and an application of the explicit expression for the Hugoniot curve, taking into account the additional features of variable cross section and external fields. So in what follows we simply list the results. The reader may consult Section 6 of [4] for more details.

Corresponding to the critical temperature T_c we have in the rarefaction fan a value β_c for which the associated RP yields,

$$T(0,\beta_c) \equiv \frac{p(0,\beta_c)}{\rho(0,\beta_c)} = T_c \ . \tag{6.6}$$

Theorem 6.1. *Let $S_\alpha(0,\beta)$, $z_\alpha(0,\beta)$ and $a(\beta) = u_\alpha(0,\beta)$ be as in Proposition 3.1 and Theorem 3.2. Then in our model we have the following expressions:*

$$(6.7)\quad S_\alpha(0,\beta) = \begin{cases} \beta^{\frac{1}{2}} S_\alpha(0,1), & \beta_c \geq 1, \\ \beta^{\frac{1}{2}}\left[S_\alpha(0,1) - K\cdot q_0 A(0)^{-1} z_- g_-^{-1} \rho_-^{1-\gamma}\cdot \frac{\gamma+1}{3\gamma-1}\left(\beta^{\frac{1-3\gamma}{\gamma+1}} - 1\right)\right], & 1>\beta\geq\beta_c, \\ \beta^{\frac{1}{2}}\cdot\beta_c^{-\frac{1}{2}} S_\alpha(0,\beta_c), & \beta<\beta_c<1, \end{cases}$$

$$(6.8)\quad S_\alpha(0,1) = \left(\frac{\partial S}{\partial \xi}\right)_- - K q_0 A(0)^{-1} z_- g_-^{-1} \rho_-^{1-\gamma}\cdot H(1-\beta_c).$$

$$(6.9)\quad z_\alpha(0,\beta) = \begin{cases} \beta^{\frac{1}{2}} z_\alpha(0,1), & \beta_c \geq 1, \\ \beta^{\frac{1}{2}}\left[z_\alpha(0,1) + K g_-^{-1} A(0)^{-1} z_-\cdot\left(\beta^{-1}-1\right)\right], & 1>\beta\geq\beta_c, \\ \beta^{\frac{1}{2}}\cdot\beta_c^{-\frac{1}{2}} z_\alpha(0,\beta_c), & \beta<\beta_c<1, \end{cases}$$

$$(6.10)\quad z_\alpha(0,1) = \left(\frac{\partial z}{\partial \xi}\right)_+ K z_- g_-^{-1} A(0)^{-1}\cdot H(1-\beta_c).$$

$$(6.11)\quad a(\beta) = a_p(\beta) + a_\phi(\beta) + a_n(\beta),$$

where, with $\lambda_- = -(\gamma-1)K q_0 z_- \rho_-\cdot H(1-\beta_c)$, (see (6.5)),

$$
(6.12)\quad a_p(\beta) = \begin{cases} a(1) - \dfrac{c_-S_-^{-1}}{(3\gamma-1)\gamma}\left(\dfrac{\partial S}{\partial \xi}\right)_-\left(\beta^{\frac{3\gamma-1}{2(\gamma+1)}}-1\right), & \beta_c \geq 1, \\[2ex] a(1) - \dfrac{\gamma(3\gamma-5)}{(3\gamma-1)^2}A(0)^{-1}g_-^{-2}\lambda_-\cdot\left(\beta^{\frac{1-3\gamma}{2(\gamma+1)}}-1\right) \\ \quad - \dfrac{\gamma-1}{3\gamma-1}g_-^{-1}\rho_-^{\gamma}\left[\left(\dfrac{\partial S}{\partial \xi}\right)_- + \dfrac{2}{3\gamma-1}\,g_-^{-1}\rho_-^{-\gamma}\lambda_-A(0)^{-1}\left(\beta^{\frac{3\gamma-1}{2(\gamma+1)}}-1\right)\right], \\ \qquad\qquad 1>\beta\geq\beta_c, \\[2ex] a(\beta_c+0) + \tfrac{1}{2}g_-^{-2}\lambda_-\beta_c^{\frac{1-3\gamma}{2(\gamma+1)}} \\ \quad - \dfrac{\gamma-1}{3\gamma-1}\,g_-^{-1}\rho_-^{\gamma}\beta_c^{-\frac{1}{2}}S_\alpha(0,\beta_c)\left[\beta^{\frac{3\gamma-1}{2(\gamma+1)}} - \beta_c^{\frac{3\gamma-1}{2(\gamma+1)}}\right], & \beta<\beta_c<1. \end{cases}
$$

$$
(6.13)\quad a_n(\beta) = -\rho_-^{-1}A(0)^{-1}n(0)\left[\frac{(\gamma-1)u_- + 2c_-}{\gamma-3}\cdot\left(\beta^{\frac{\gamma-3}{2(\gamma+1)}}-1\right) - \frac{4c_-}{3\gamma-5}\cdot\left(\beta^{\frac{3\gamma-5}{2(\gamma+1)}}-1\right)\right],
$$

$$
(6.14)\quad a_\phi(\beta) = A(0)^{-1}g_-^{-1}\phi'(0)\left(\beta^{-\frac{1}{2}}-1\right).
$$

Remarks 6.2. (a) Observe that $a_p(\beta), a_n(\beta)$ and $a_\phi(\beta)$ reflect, respectively, the planar part, the contribution due to the variable cross section $\left(n(0) = \frac{A'(0)}{A(0)}\right.$ by (2.7)$\left.\right)$ and the contribution due to the external field.

(b) It is interesting that the expression (6.13) for $a_n(\beta)$ is singular for $\gamma = 3, \frac{5}{3}$. For these two values one obtains the correct expressions by taking the analytic limits as $\gamma \to 3$ or $\gamma \to \frac{5}{3}$ (compare [3]).

(c) The case $\beta_c \geq 1$ means simply that there is no chemical reaction throughout the whole rarefaction wave, since clearly the temperature decreases in the direction of decreasing β.

Recall that by (4.3) the coefficients a_-, b_- and d_- in (4.1) are known once $a(\beta)$ (and the solution of the associated RP) are known. Thus, it remains to derive explicit expressions for a_+, b_+ and d_+. In this setting (Fig.1) we are assuming that there is a shock wave travelling to the right. Obviously, the Hugoniot (p-u) relation for this shock is not affected by the variable cross section and the presence of an external potential. However the transition from spatial to time derivatives (and vice versa) involves these two additional ingredients. Thus, the method of derivation for the formulae in the following theorem is identical with that of Section 6 in [4], but there are additional terms.

Theorem 6.3. *Assume the wave configuration of Figure 1 as well as (6.1),(6.3) for the equation of state and the reaction rate. Then the coefficients a_+, b_+, d_+ in (4.2) are given by the following expressions, where $W_+ = A(0)\frac{p^*-p_+}{u^*-u_+}$ is the (Lagrangian) speed of the shock, $\mu^2 = \frac{\gamma-1}{\gamma+1}$, and $n(0) = \frac{A'(0)}{A(0)}$.*

$$(6.15) \qquad a_+ = 2 - \frac{1}{2}\frac{p^*-p_+}{p^*+\mu^2 p_+},$$

$$(6.16) \qquad b_+ = \frac{1}{2}\frac{u^*-u_+}{p^*+\mu^2 p_+} - (g_+^*)^{-2}A(0)^{-1}W_+ - A(0)W_+^{-1},$$

$$(6.17) \qquad d_+ = L_u\left(\frac{\partial u}{\partial \xi}\right)_+ + L_p\left(\frac{\partial p}{\partial \xi}\right)_+ + L_\rho\left(\frac{\partial \rho}{\partial \xi}\right)_+ + L_\lambda + L_n \cdot n(0) + L_\phi \cdot \phi'(0),$$

where,

$$(6.18) \qquad L_u = \frac{A(0)}{2}(u^*-u_+)\left[\rho_+ + \frac{\mu^2 g_+^2}{p^*+\mu^2 p_+}\right] + g_+^2 A(0)^2 W_+^{-1} + W_+,$$

$$(6.19)\qquad L_p = -A(0)\left[2 + \frac{\mu^2}{2}\,\frac{p^*-p_+}{p^*+\mu^2 p_+}\right],$$

$$(6.20)\qquad L_\rho = -\frac{W_+}{2\rho_+}(u^*-u_+),$$

$$(6.21)\qquad L_n = \frac{u^*-u_+}{2}\left[u_+ + \frac{\mu^2 g_+ c_+ u_+}{p^*+\mu^2 p_+}\right] + A(0)W_+^{-1}u_+c_+g_+ + A(0)^{-1}W_+u^*(\rho_+^*)^{-1},$$

$$(6.22)\qquad L_\lambda = \lambda_+\left[A(0)W_+^{-1} + \frac{\mu^2}{2}\,\frac{u^*-u_+}{p^*+\mu^2 p_+}\right] + \lambda_+^* \cdot A(0)^{-1}W_+(g_+^*)^{-2},$$

$$\lambda_+ = \lambda(\rho_+, p_+, z_+), \quad \lambda_+^* = \lambda(\rho_+^*, p^*, z_+) \quad \text{(see (6.5))},$$

$$(6.23)\qquad L_\phi = -2 + \frac{p^*-p_+}{2(p^*+\mu^2 p_+)}.$$

This concludes the discussion of the special case. The formulae of this section enable one to work in the context of the Lagrangian solution of the GRP (Section 4) or the Eulerian solution (Section 5) with fully explicit expressions for the fluxes. Our numerical examples in the next section are all built on this special case.

7. *Numerical Examples*

The GRP scheme is based on a direct application of the analytic solution at cell-boundaries, as outlined in the Introduction, Equations (1.2) and (1.5). However, using the special case of Section 6 we have a non-smooth reaction rate, involving a jump discontinuity at the critical temperature T_c (see Eq. (6.3)). Hence some care is needed when discretizing the fourth equation in (1.1).

Let us summarize briefly the steps taken in the implementation of the GRP method.

We assume that at time $t = t_n = n\Delta t$ we are given all cell averages U_i^n as well as the variations $(\Delta U)_i^n$. These can be translated into either Lagrangian or Eulerian (constant) slopes using (2.6). We now proceed as follows.

Step 1. At each cell boundary the GRP is solved according to Section 5 and $U_{i+\frac{1}{2}}^{n+\frac{1}{2}}$ is evaluated as in (1.5). Then the fluxes $F(U)_{i+\frac{1}{2}}^{n+\frac{1}{2}}$, $G(U)_{i+\frac{1}{2}}^{n+\frac{1}{2}}$ are determined.

Step 2. Using the difference scheme (1.2) for the first two equations in (1.1), the new densities and velocities ρ_i^{n+1} and u_i^{n+1} are calculated.

Step 3. The source term for the chemistry equation (the fourth component of $H(U_i^{n+\frac{1}{2}})$ in (1.2)) is calculated as follows (we are using the special form (6.3) and the solution $U_{i+\frac{1}{2}}^{n+\frac{1}{2}}$ to the GRP).

$$(7.1)\qquad (\widetilde{k\rho})_i^{n+\frac{1}{2}} = \tfrac{1}{2}K\left[(\rho z)_{i+\frac{1}{2}}^{n+\frac{1}{2}} \cdot H(T_{i+\frac{1}{2}}^{n+\frac{1}{2}} - T_c) + (\rho z)_{i-\frac{1}{2}}^{n+\frac{1}{2}} \cdot H(T_{i-\frac{1}{2}}^{n+\frac{1}{2}} - T_c)\right].$$

Step 4. The third and fourth equations in (1.2) are then solved

simultaneously, thus obtaining the first approximations $\tilde{z}_i^{n+1}, \tilde{e}_i^{n+1}$ and hence also $\tilde{p}_i^{n+1}$ and $\tilde{T}_i^{n+1}$. Here we are using (7.1) for the fourth equation.

Step 5. A new source term for the chemistry equation is determined by

$$(7.2) \qquad (k\rho)_i^{n+\frac{1}{2}} = (\widetilde{k\rho})_i^{n+\frac{1}{2}} \cdot H\left(\frac{\tilde{T}_i^{n+1} + T_i^n}{2} - T_c\right).$$

Step 6. If in (7.2) $(k\rho)_i^{n+\frac{1}{2}} \neq (\widetilde{k\rho})_i^{n+\frac{1}{2}}$, we repeat Step 4 with the new source term $(k\rho)_i^{n+\frac{1}{2}}$ thus obtaining final results for p_i^{n+1}, z_i^{n+1}, e_i^{n+1}.

Step 7. The new variations in cells are determined by,

$$(7.3) \qquad (\Delta U)_i^{n+1} = U_{i+\frac{1}{2}}^{n+1} - U_{i-\frac{1}{2}}^{n+1},$$

and a simple monotonicity algorithm is applied [1,15].

This concludes the discussion of the scheme and we can now proceed to discuss concrete numerical examples. We have made an attempt to exhaust the various combinations of ingredients in (1.1), namely, chemical reactions, variable cross section and external fields. Table II lists those ingredients included in each example.

Table II — Various ingredients in the numerical examples

example	external field	chemistry	variable cross section
1	—	—	Yes
2	—	Yes	Yes
3(a)	Yes	—	Yes
3(b)	Yes	Yes	Yes

As a rule, we work with a constant time-step Δt in all examples. This forces a relatively low CFL number. Of course, the presence of a "stiff" reaction rate and our explicit discretization of the chemistry equation also require a low CFL number.

Example 1. *(Infinite Reflected Shock).* As our first example we take a test problem involving an infinite reflected shock in spherical geometry, proposed by W.F. Noh [13] in an unpublished memorandum.

An infinite sphere of gas is initially cold with pure kinetic energy. Thus, the equation-of-state (6.1) is used with $\gamma = \frac{5}{3}$ and the initial (uniform) values for the thermodynamic variables are (in any convenient units),

$$\rho = 1, \qquad p = 0.$$

At time $t = 0$ the gas is uniformly imploding with velocity $u = -1$.

Clearly the initial conditions imply that at $t = 0$ an infinite shock is reflected from the origin and brings the incoming gas to rest. Since the infinite shock compression is $\frac{\gamma+1}{\gamma-1} = 4$ it follows directly from the Rankine-Hugoniot conditions that the (uniform) speed of the reflected shock is $W = \frac{1}{3}$. At time $t = 3$ it reaches the radius $r = 1$ where it encounters fluid particles that originated at $r = 4$. Hence the (uniform) density behind the shock is given by $\frac{4\pi}{3}\bar{\rho} = \frac{4\pi}{3} \cdot 4^3$, that is, $\bar{\rho} = 64$. The Rankine-Hugoniot condition now implies that the (uniform) pressure behind the shock is $p = \frac{64}{3}$. The velocity and pressure profiles ahead of the shock are equal to their initial values. The density varies due to geometrical compression. The spherical shell of width dr, initially located at $r \geq \frac{4}{3}t$, reaches the radius r-t at time t, so that $4\pi r^2 dr = 4\pi\rho(r,t)(r-t)^2 dr$, whence,

$$\rho(r-t,t) = \frac{r^2}{(r-t)^2}, \qquad r \geq \frac{4}{3}t .$$

This concludes the analytic solution for this problem. In the calculation we took 100 (Eulerian) points equally spaced with $\Delta r = 1$. We used a time step of $\Delta t = 0.25$. The results after 900 time steps ($t = 225$)

are shown in Figure 2. The solid line gives the exact solution while the dots represent the calculated quantities. It is seen that the average calculated density is 63.14 (compared with 64 for the exact one). The location of the shock is obtained with very high accuracy, and so is the density profile ahead of the shock.

Figure 2

Example 2. *(Taylor Blast Wave).* In this example we calculate the flow profiles behind a spherical detonation wave initiated at the origin r=0. We assume that the explosion propagates into a uniform unburnt gas at rest, where $p = p_0$, $\rho = \rho_0$.

Using the Chapman-Jouguet model (namely, a sharp reaction front) and the assumption that the outward blast wave travels at the C-J speed, G.I. Taylor [14] has shown that the solution is self-similar in the sense that all quantities depend on $\frac{r}{t}$ only. Thus, the system (1.1) is reduced to a set of coupled ordinary differential equations in terms of the similarity coordinate $x = \frac{r}{t}$.

In our numerical treatment we started (at t=0) with Taylor's profile where the shock is located at x = 2. We are using 100 (Eulerian) points equally distributed over the interval $0 \leq x \leq 10$, and take a constant time step $\Delta t = 4.10^{-3}$ μsec. Following Taylor, we take in the unburnt gas ahead of the shock,

$$p_0 = 1.0135 \cdot 10^{-6} \text{ Mbar}, \qquad \rho_0 = 1.51 \ \frac{\text{gr}}{\text{cm}^3}.$$

For both the burnt and unburnt gas we take the same equation-of-state (6.1)

with

$$\gamma = 3.09, \qquad q_0 = .2381 \cdot 10^{-1} \ \frac{\text{Mbar cm}^3}{\text{gr}} .$$

For the reaction rate we take the simplified Arrhenius model (6.3), with $T_C = .13245 \cdot 10^{-1} \ \frac{\text{Mbar cm}^3}{\text{gr}}$ (recall that $T = \frac{p}{\rho}$).

Our calculations were carried out for 2500 time steps, up to t = 10 μsec, using two different values for K in (6.3).

(a) $K = 159.5 \ \mu\text{sec}^{-1} \qquad \left(= 25 \cdot \frac{U_{CJ}}{\Delta x} \right)$,

(b) $K = 254.2 \ \mu\text{sec}^{-1} \qquad \left(= 40 \cdot \frac{U_{CJ}}{\Delta x} \right)$.

The resulting profiles are shown in Figures 3(a) and 3(b) respectively. The solid line represents Taylor's exact solution (C-J model).

Note that while Taylor's solution is obtained by assuming the Chapman-Jouguet theory as well as a C-J uniform shock speed, the reaction rates in the numerical calculation are finite. Thus there is no apriori reason to assume that the reaction zone should move at exactly the C-J speed.

Figure 3(a)

Figure 3(b)

Example 3. *(Gas in Cluster).* This problem is taken from [16]. We consider a uniform gas, initially at rest, and subject to an external potential of the form,

$$\phi(r) = - (1+r^2)^{-\frac{1}{2}} .$$

The gas starts to collapse under the external force (directed inward) and pressure, density and temperature begin to rise. We shall now examine what happens in two cases: (a) Non-reactive flow; (b) Reactive flow. In both cases the uniform initial values (in any convenient units) are,

$$p_0 = 0.0067, \qquad \rho_0 = 1.$$

The equation-of-state is (6.1) with $\gamma = \frac{5}{3}$.

In both cases we are using an equally spaced (Eulerian) grid of 100 cells with $\Delta r = 0.03$. Non reflective boundary conditions are applied at $r = 3$.

Case (a): Non-reactive flow. As the pressure gradient builds up, a shock is formed close to the center (Figure 4(a) where only the first 67 cells are shown), bringing the collapsing gas to a halt. At this point

---

Figure 4(a)

---

the density near the center increases by a factor of about 100, while the pressure there is about 2000 times its initial magnitude. In Figure 4(b) we show the flow profiles at $t = 4$. The outgoing shock is very sharp and the calculated profiles are very smooth. Our results here are in good agreement with those obtained by Yahil et al [16].

Figure 4(b)

Case (b): Reactive flow. The initial conditions here are the same as in Case (a), but the gas is reactive. The equation-of-state is again (6.1), with

$$\gamma = \frac{5}{3}, \qquad q_0 = 5,$$

and the reaction rate is given by (6.3), with

$$K = 20, \qquad T_c = 0.1.$$

Note that our reaction equation is different from that of [16].

The initial stages of the flow are similar to those of Case (a). However, as the gas collapses it heats up and the temperature near the center rises above T_c. At this point the gas is ignited and brought to a halt. This happens approximately at t = 1.55, much earlier than the formation of the fluid dynamical shock in Case (a). Figure 5(a) shows the flow profiles at this time, just before ignition. The subsequent flow is of course very different from that of the former case. In Figure 5(b) we plot the flow profiles at t = 1.6 just after ignition. The density is about 55 times its original value, while the pressure is around 10,500 times its original value p_o. Thus, compared to the non-reactive case, the temperatures reached here are much higher (in the temperature graph the critical temperature T_c is marked by a horizontal line). In Figure 5(c) we show the flow at a later stage t = 2.4. Note the change of scale between Figures 5(b) and 5(c). We observe that the outgoing wave consists of a precompressive shock followed by a reaction zone which occupies about 10 cells. As in the previous case the shock is sharp and the profiles behind it are smooth. Even though our reaction equation is not identical with that of [16] (and the calculation there is Lagrangian), our results are qualitatively in good agreement with those obtained there.

Figure 5(a)

Figure 5(b)

Figure 5(c)

Appendix

Following Theorem 4.1, we stated that once the time derivatives $(\frac{\partial V}{\partial t})^*$ are known (along a contact discontinuity), the spatial derivatives $(\frac{\partial V}{\partial \xi})^*_{\pm}$ can be evaluated. The method of derivation is identical to that of Section 4 in [4], but extra terms appear as a result of the additional external fields and variable cross section. We are using the wave-configuration of Figure 1.

Derivatives behind the shock ($W_+ = A(0) \cdot \frac{p^*-p_+}{u^*-u_+}$ = ***Lagrangian shock speed***)

$$(A.1)\quad (\frac{\partial p}{\partial \xi})^*_+ = - A(0)^{-1}\left[(\frac{\partial u}{\partial t})^* + \phi'(0)\right],$$

$$(A.2)\quad (\frac{\partial u}{\partial \xi})^*_+ = - A(0)^{-1}(g^*_+)^{-2}\left[(\frac{\partial p}{\partial t})^* + \lambda(\rho^*_+, e^*_+, z^*_+)\right] - A(0)^{-1}(\rho^*_+)^{-1} \cdot n(0)u^*,$$

$$n(0) = \frac{A'(0)}{A(0)} .$$

$$(A.3)\quad (\frac{\partial z}{\partial \xi})^*_+ = (\frac{\partial z}{\partial \xi})_+ + W_+^{-1} \cdot \left[k(\rho^*_+, e^*_+, z_+) - k(e_+, \rho_+, z_+)\right] \text{ (with k as in (1.1))}.$$

$$(A.4)\quad (\frac{\partial \rho}{\partial \xi})^*_+ = - \left[3W_+^{-1}(c^*_+)^{-2} + A(0)^2(\rho^*_+)^2 W_+^{-3}\right](\frac{\partial p}{\partial t})^* + 3A(0)(\rho^*_+)^2 W_+^{-2}(\frac{\partial u}{\partial t})^*$$

$$+ 3A(0)^2(\rho^*_+)^2 W_+^{-2}(\frac{\partial p}{\partial \xi})_+ + (\rho^*_+)^2 \rho_+^{-2}(\frac{\partial \rho}{\partial \xi})_+$$

$$- \left[3W_+ + A(0)^2 g_+^2 W_+^{-1}\right] \cdot A(0)(\rho^*_+)^2 W_+^{-2}(\frac{\partial u}{\partial \xi})_+$$

$$- \left[3W_+^{-1}(c^*_+)^{-2}\lambda(\rho^*_+, e^*_+, z_+) - A(0)^2(\rho^*_+)^2 W_+^{-3}\lambda(\rho_+, e_+, z_+)\right]$$

$$+ 3A(0)(\rho^*_+)^2 W_+^{-2}\phi'(0) -$$

$$- A(0)(\rho^*_+)^2 W_+^{-2}\left[A(0)W_+^{-1}g_+^2 u_+ \rho_+^{-1} + A(0)^{-1}u_+ W_+ \rho_+^{-1} + 2W_+ A(0)^{-1}(\rho^*_+)^{-1}u^*\right] \cdot n(0).$$

Derivatives behind the rarefaction wave

Here we list the derivatives $(\frac{\partial Q}{\partial \xi})^*_-$ behind a rarefaction wave (in the configuration of Figure 1). They are obtained either from the equations (2.7) or from the directional derivatives $\frac{\partial Q}{\partial \alpha}(0,\beta^*)$ along the tail characteristic of the rarefaction fan. In the latter case one simply uses the chain rule,

$$(A.5)\qquad \frac{\partial Q}{\partial \alpha}(0,\beta^*) = (\frac{\partial Q}{\partial \xi})^*_- \cdot \frac{\partial \xi}{\partial \alpha}(0,\beta^*) + (\frac{\partial Q}{\partial t})^*_- (\frac{\partial t}{\partial \alpha})(0,\beta^*)$$

$$= (\frac{\partial Q}{\partial \xi})^*_- \cdot (\beta^*)^{\frac{1}{2}} - (\frac{\partial Q}{\partial t})^*_- \cdot g_-^{-1}A(0)^{-1}(\beta^*)^{-\frac{1}{2}}$$

(see Equation (3.4)). The derivative $\frac{\partial Q}{\partial \alpha}(0,\beta^*)$ is known from Theorem 3.2 and Corollary 3.3, while $(\frac{\partial Q}{\partial t})^*_-$ (along the left-hand side of the contact discontinuity) is known from the analysis of Section 4. Thus (A.5) can be solved for $(\frac{\partial Q}{\partial \xi})^*_-$. This method applies especially for the case of $(\frac{\partial \rho}{\partial \xi})^*_-$, which cannot be recovered from the system (2.7).

We list the relevant formulae,

$$(A.6)\qquad (\frac{\partial p}{\partial \xi})^*_- = - A(0)^{-1}\Big[(\frac{\partial u}{\partial t})^* + \phi'(0)\Big],$$

$$(A.7)\qquad (\frac{\partial u}{\partial \xi})^*_- = - A(0)^{-1}(g_-^*)^{-2}\Big[(\frac{\partial p}{\partial t})^* + \lambda(\rho_-^*, e_-^*, z_-)\Big] - A(0)^{-1}(\rho_-^*)^{-1}u^* \cdot n(0),$$

$$(A.8)\qquad (\frac{\partial \rho}{\partial \xi})^*_- = (\beta^*)^{-\frac{1}{2}}(\frac{\partial \rho}{\partial \alpha})(0,\beta^*) + A(0)^{-1}(g_-^*)^{-1}(\frac{\partial \rho}{\partial t})^*_- .$$

References

[1] M. Ben-Artzi and J. Falcovitz, A second order Godunov-type scheme for compressible fluid dynamics, *J. Comp. Phys.* 55 (1984), 1-32.

[2] M. Ben-Artzi and J. Falcovitz, A high-resolution upwind scheme for quasi 1-D flows, in *Numerical Methods for the Euler Equations of Fluid Dynamics*, F. Angrand, A. Dervieux, J.A. Desideri and R. Glowinski (Editors), SIAM Publ., 1985, 66-83.

[3] M. Ben Artzi and J. Falcovitz, An upwind second-order scheme for compressible duct flows, *SIAM J. Sci. Stat. Comp.* 7 (1986), 744-768.

[4] M. Ben-Artzi, The generalized Riemann problem for reactive flows, *J. Comp. Phys.* (to appear).

[5] A. Bourgeade, Second order scheme for reactive flow. Application to detonation (preprint).

[6] A. Bourgeade, P. Le Floch and P.A. Raviart, Approximate solution of the generalized Riemann problem and applications, in *Nonlinear Hyperbolic Problems*, C. Carasso, P.A. Raviart and D. Serre (Editors), 1-9. Lecture Notes in Mathematics # 1270, Springer-Verlag 1987.

[7] P. Colella, A. Majda and V. Roytburd, Theoretical and numerical structure for reacting shock waves, *SIAM J. Sci. Stat. Comp.* 7 (1986), 1059-1080.

[8] R. Courant and K.O. Friedrichs, *Supersonic Flow and Shock Waves*, Interscience, New York, 1949.

[9] S.K. Godunov, A finite difference method for the numerical computation of discontinuous solutions of the equations of fluid dynamics, *Mat. Sb.* 47 (1959), 271-295.

[10] E. Harabetian, *A Cauchy-Kowalevsky theorem for strictly hyperbolic systems of conservation laws with piecewise analytic initial data*, Ph.D. Thesis, UCLA, 1984.

[11] P. Le Floch and P.A. Raviart, An asymptotic expansion for the solution of the generalized Riemann problem, Ecole Polytechnique Preprint #160, 1987.

[12] T. Li and W. Yu, *Boundary Value Problems for Quasilinear Hyperbolic Systems*, Duke University Mathematics Series, 1985.

[13] W.F. Noh, Unpublished memorandum, Lawrence Livermore Laboratory, Univ. of California, 1982.

[14] G.I. Taylor, The dynamics of the combustion products behind plane and spherical detonation fronts in explosives, in *The Scientific Papers of G.I. Taylor, Vol.III*, G.K. Bathchelor (Ed.) pp. 465-478, Cambridge Univ. Press, 1963.

[15] B. van-Leer, Towards the ultimate conservative difference scheme, V, *J. Comp. Phys.* 32, (1979), 101-136.

[16] A. Yahil, M.D. Johnston and A. Burrows, A conservative Lagrangian hydrodynamical scheme with parabolic spatial accuracy, submitted to the *J. Comp. Phys.*

Figure Captions

Figure 1 Setup for the generalized Riemann problem

Figure 2 Reflection of spherical infinite shock

Figure 3(a) Taylor explosion profile: $K = 159.5\ \mu sec^{-1}$

Figure 3(b) Taylor explosion profile: $K = 254.2\ \mu sec^{-1}$

Figure 4(a) Non-reactive collapsing gas: Shock is formed

Figure 4(b) Non-reactive collapsing gas: A sharp shock is moving out

Figure 5(a) Reactive collapsing gas, shortly before ignition

Figure 5(b) Reactive collapsing gas, shortly after ignition

Figure 5(c) Reactive collapsing gas, when most of the gas is burnt out

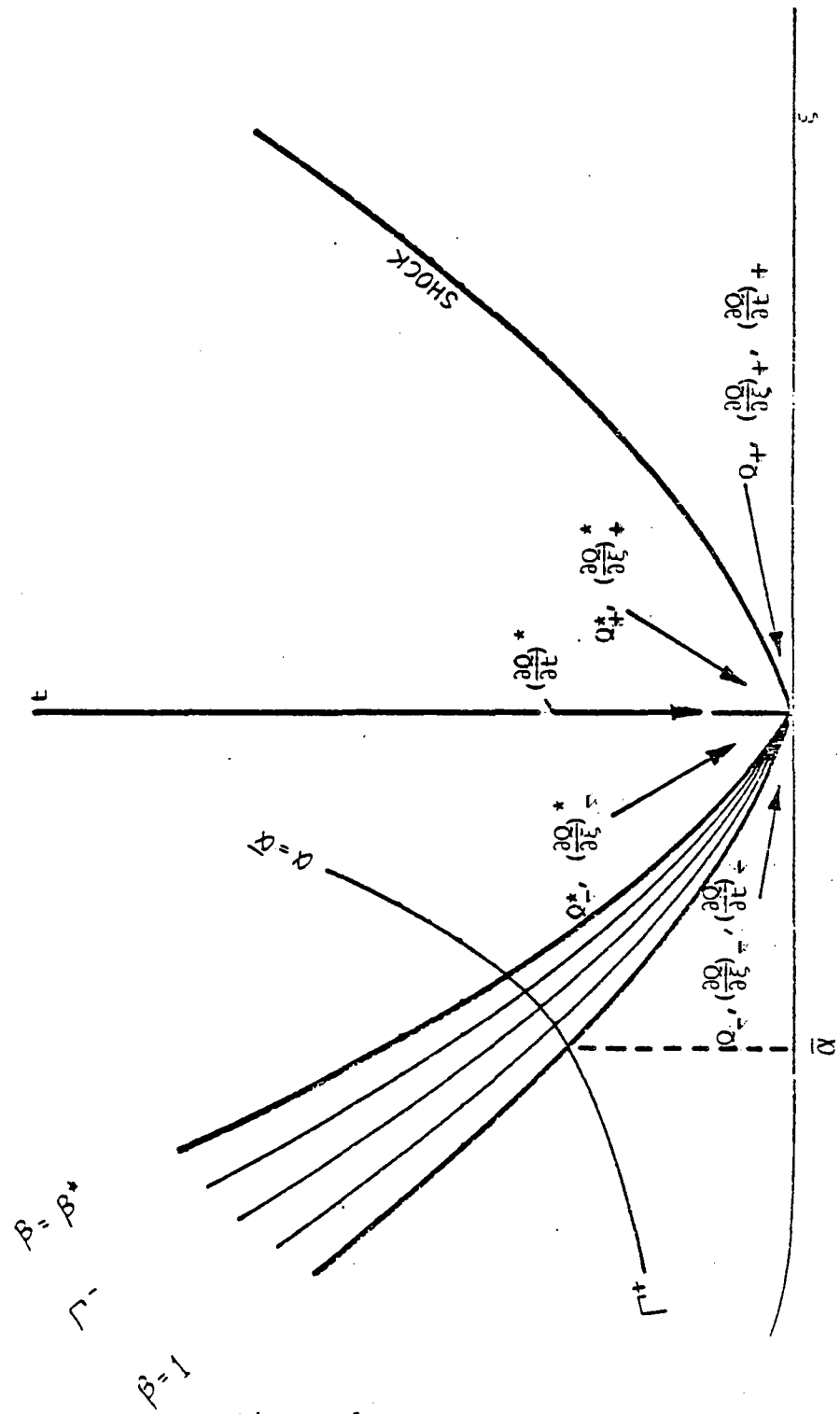
SHOCK
$\beta = \beta^*$
$\beta = 1$
$\alpha = \alpha_1$
ξ
$\bar{R}$
η
$\left(\frac{\partial \theta}{\partial \xi}\right)^*_1$
$\left(\frac{\partial \theta}{\partial \eta}\right)^*$
$\left(\frac{\partial \theta}{\partial \xi}\right)^*$
α^*_+
α^*_-
α_+
α_-
$\left(\frac{\partial \eta}{\partial \theta}\right)_+$
$\left(\frac{\partial \xi}{\partial \theta}\right)_+$
$\left(\frac{\partial \eta}{\partial \theta}\right)_-$
$\left(\frac{\partial \xi}{\partial \theta}\right)_-$

Figure 1

NOH'S FIRST PROBLEM

L= 100. DX= 1.000 DT= .25000

GAMA= 1.67
CFLMAX= .311

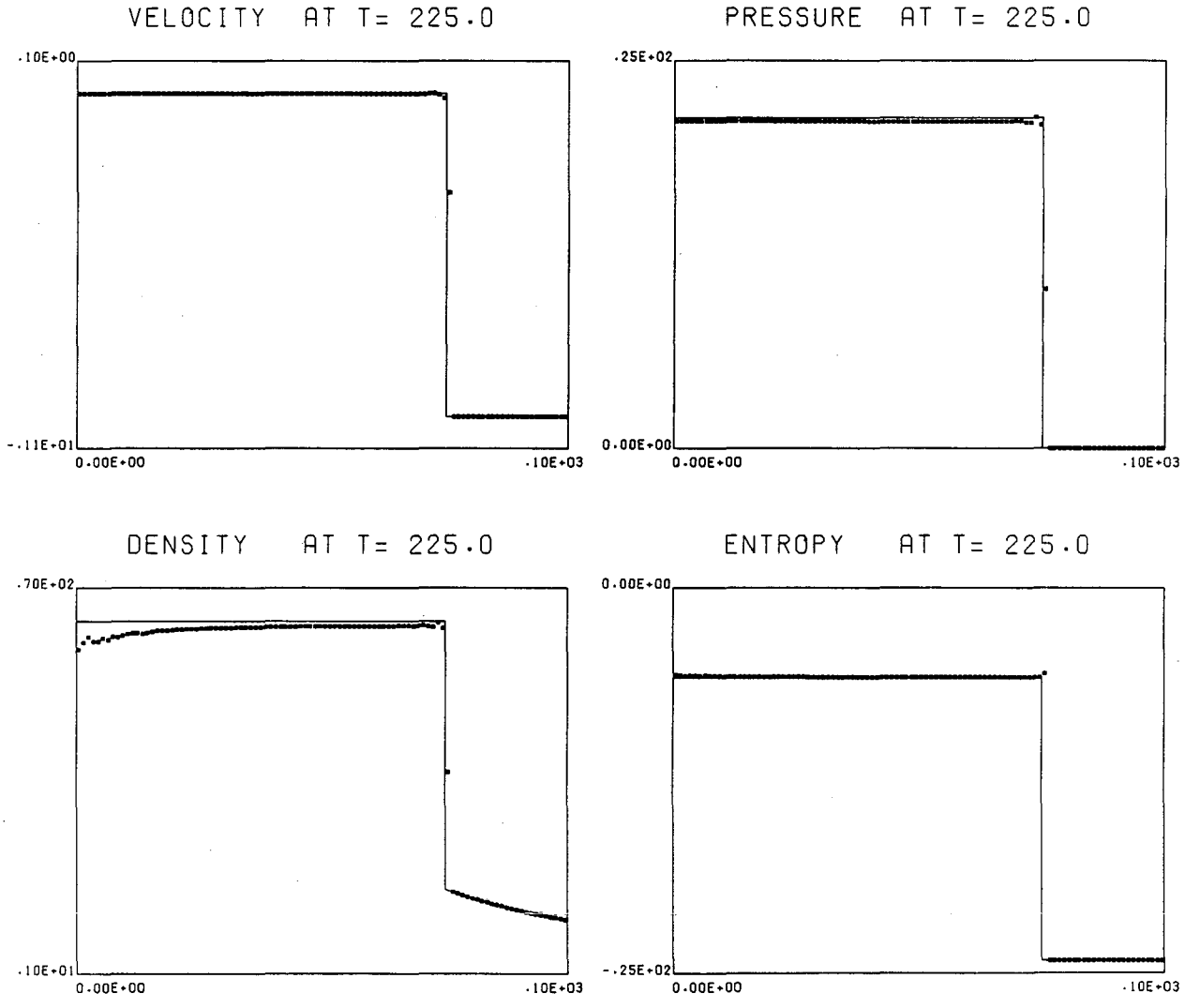

Figure 2

L= 100. DX= .1000E+00 DT= .40000E-02
EXPLICIT=.TRUE . TC= .132E-01RATE= 25.00 *DCJ/DX
GAMA= 3.09
CFLMAX= .231E-01 D= .60948

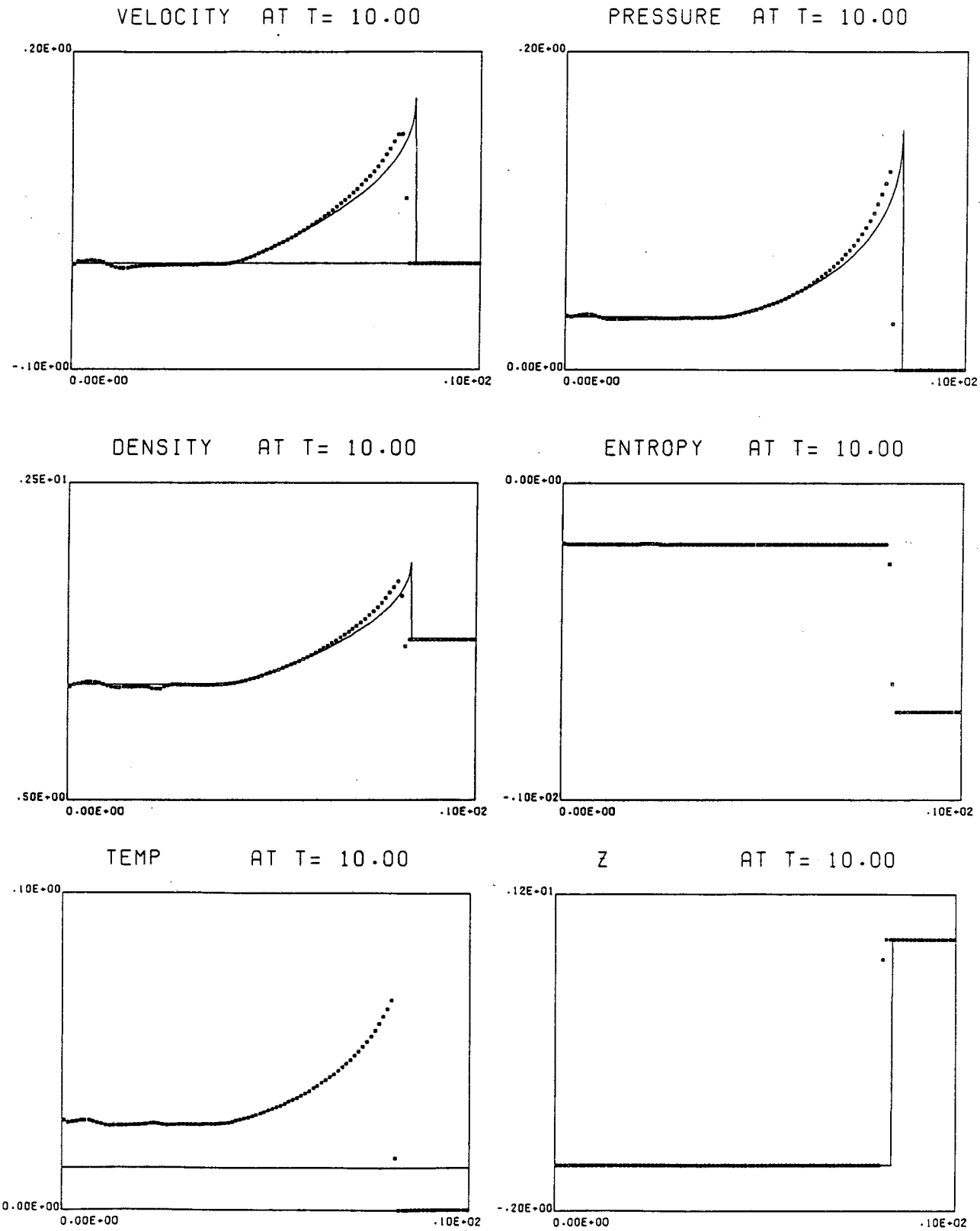

Figure 3(a)

L= 100. DX= .1000E+00 DT= .40000E-02
EXPLICIT=.TRUE . TC= .132E-01RATE= 40.00 *DCJ/DX
GAMA= 3.09
CFLMAX= .225E-01 D= .66008

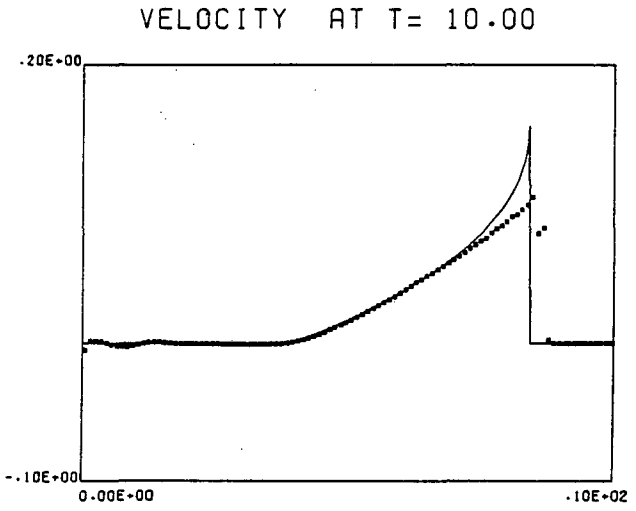

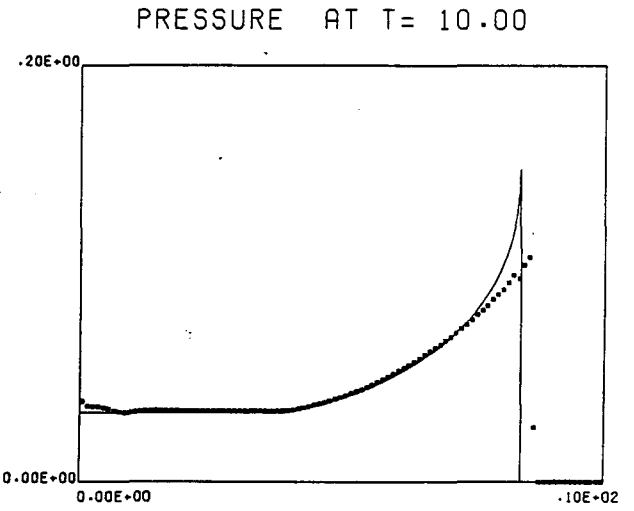

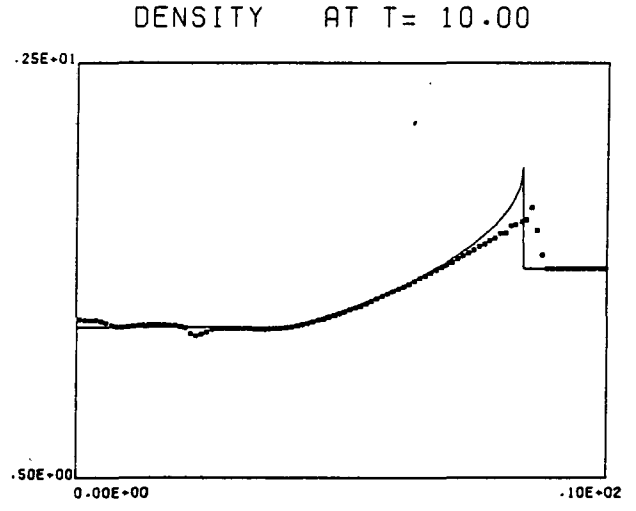

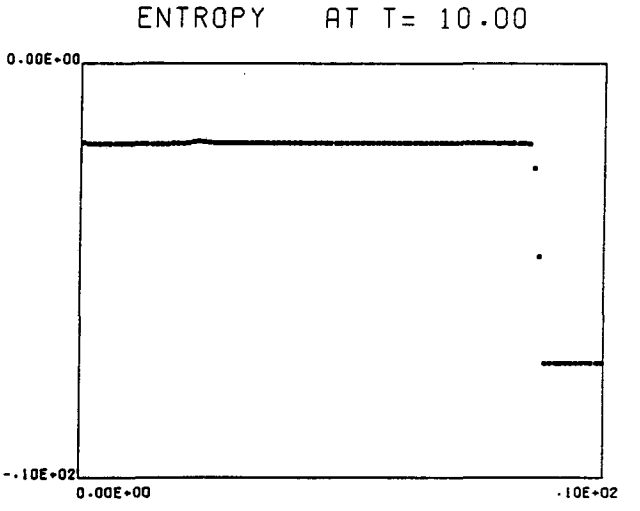

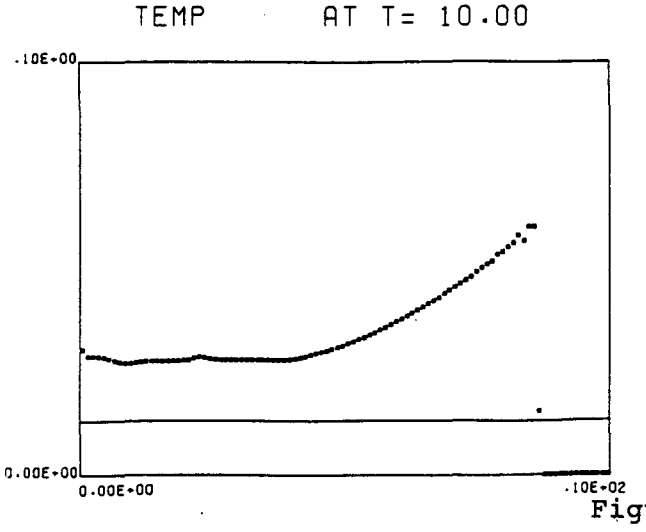

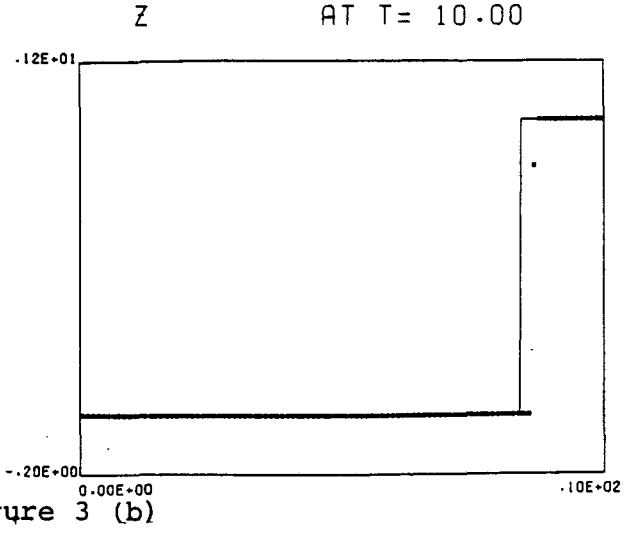

Figure 3 (b)

GAS COLLAPSE UNDER POTEN=-1/SQRT(1+R**2)
(NO MICROPHYSICS)

L= 100. DX= .3000E-01 DT= .50000E-02

GAMA= 1.67
CFLMAX= .145

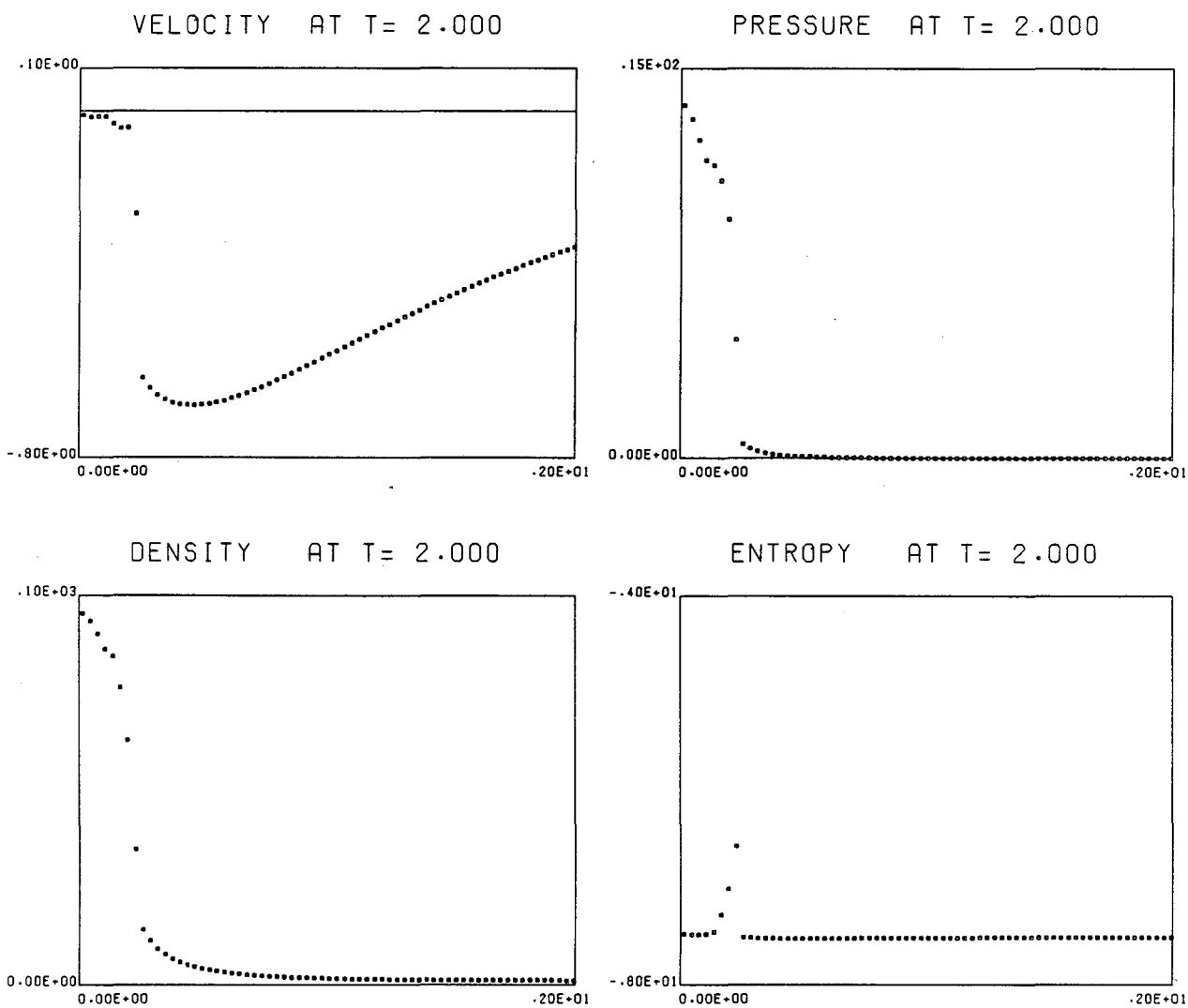

Figure 4 (a)

GAS COLLAPSE UNDER POTEN=-1/SQRT(1+R**2)
(NO MICROPHYSICS)

L= 100. DX= .3000E-01 DT= .50000E-02

GAMA= 1.67
CFLMAX= .167

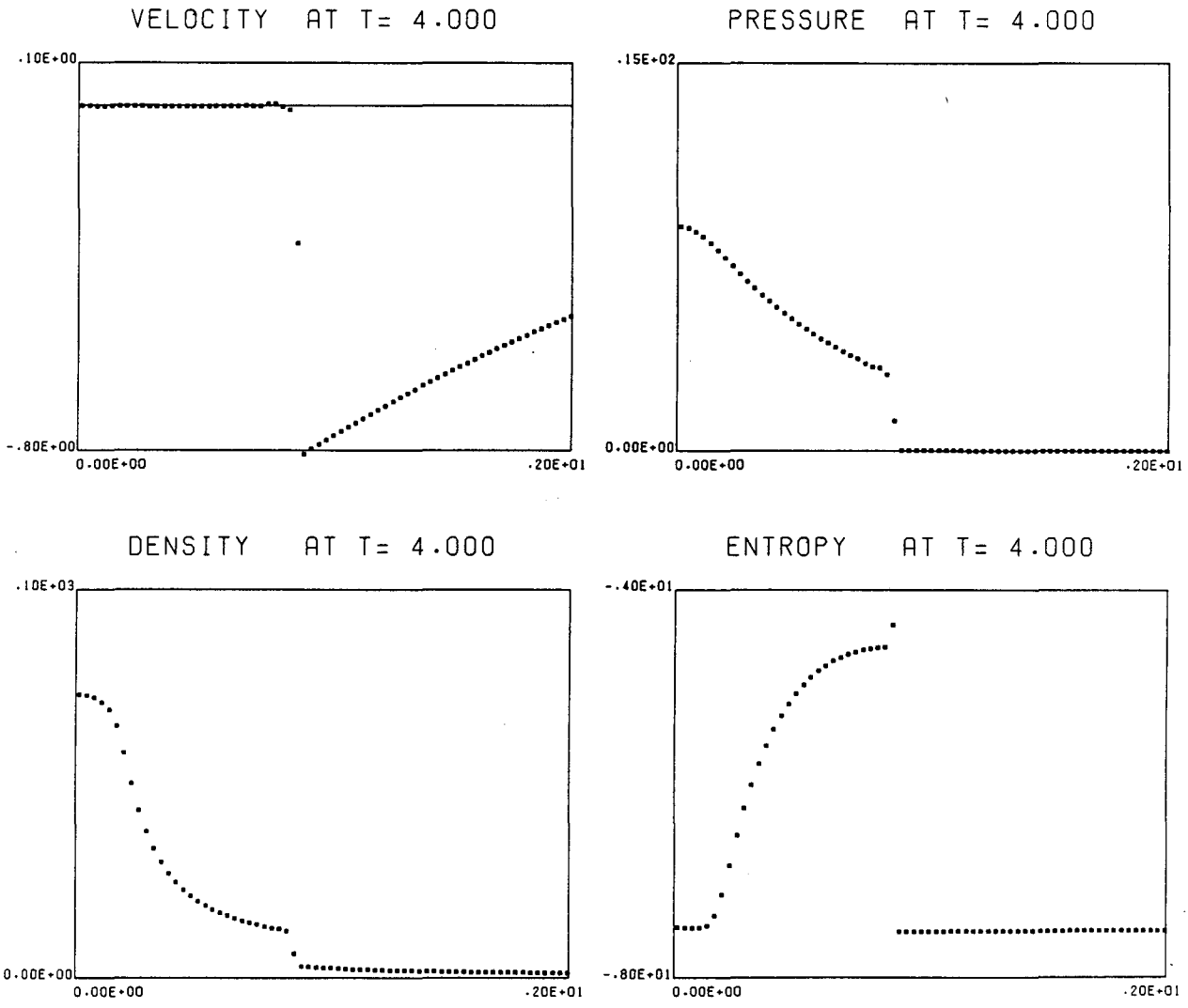

Figure 4 (b)

GAS COLLAPSE UNDER POTEN=-1/SQRT(1+R**2)
(WITH MICROPHYSICS)

L= 100. DX= .3000E-01 DT= .10000E-02
EXPLICIT=.TRUE . TC= .100 RATE= 20.0
GAMA= 1.67
CFLMAX= .240E-01

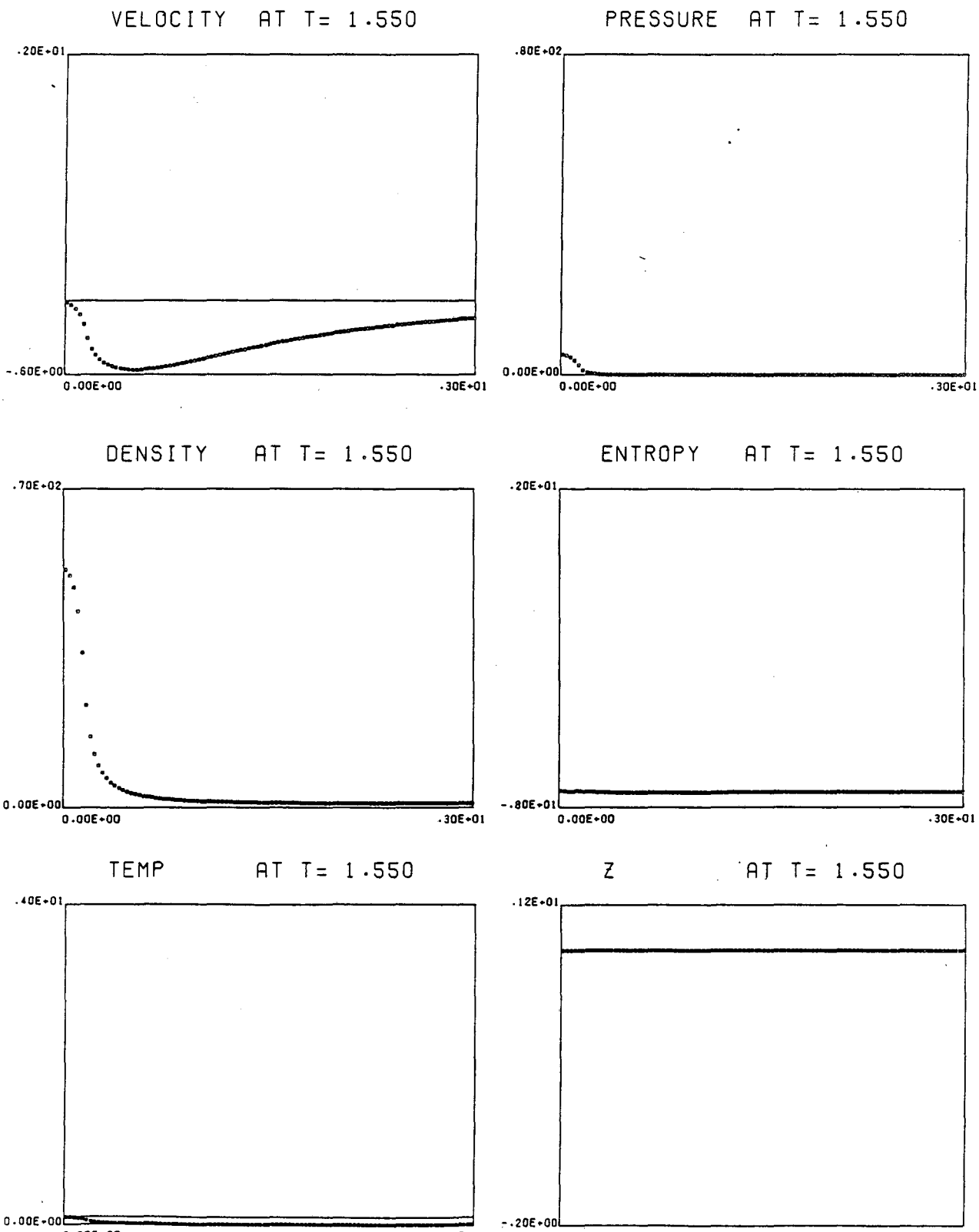

Figure 5 (a)

GAS COLLAPSE UNDER POTEN=-1/SQRT(1+R**2)
(WITH MICROPHYSICS)

L= 100. DX= .3000E-01 DT= .10000E-02
EXPLICIT=.TRUE . TC= .100 RATE= 20.0
GAMA= 1.67
CFLMAX= .483E-01

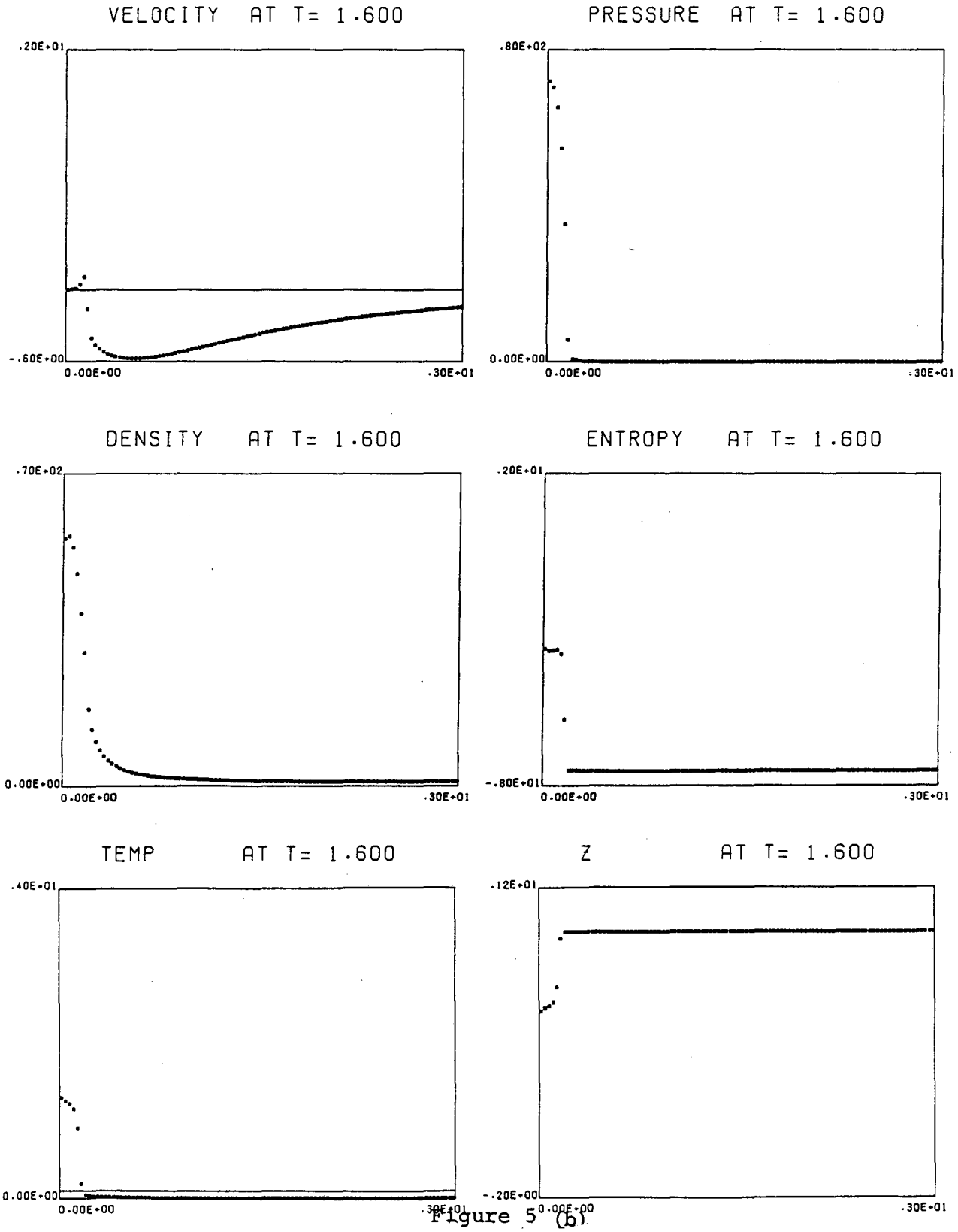

Figure 5 (b)

GAS COLLAPSE UNDER POTEN=-1/SQRT(1+R**2)
(WITH MICROPHYSICS)

L= 100. DX= .3000E-01 DT= .10000E-02
EXPLICIT=.TRUE . TC= .100 RATE= 20.0
GAMA= 1.67
CFLMAX= .131

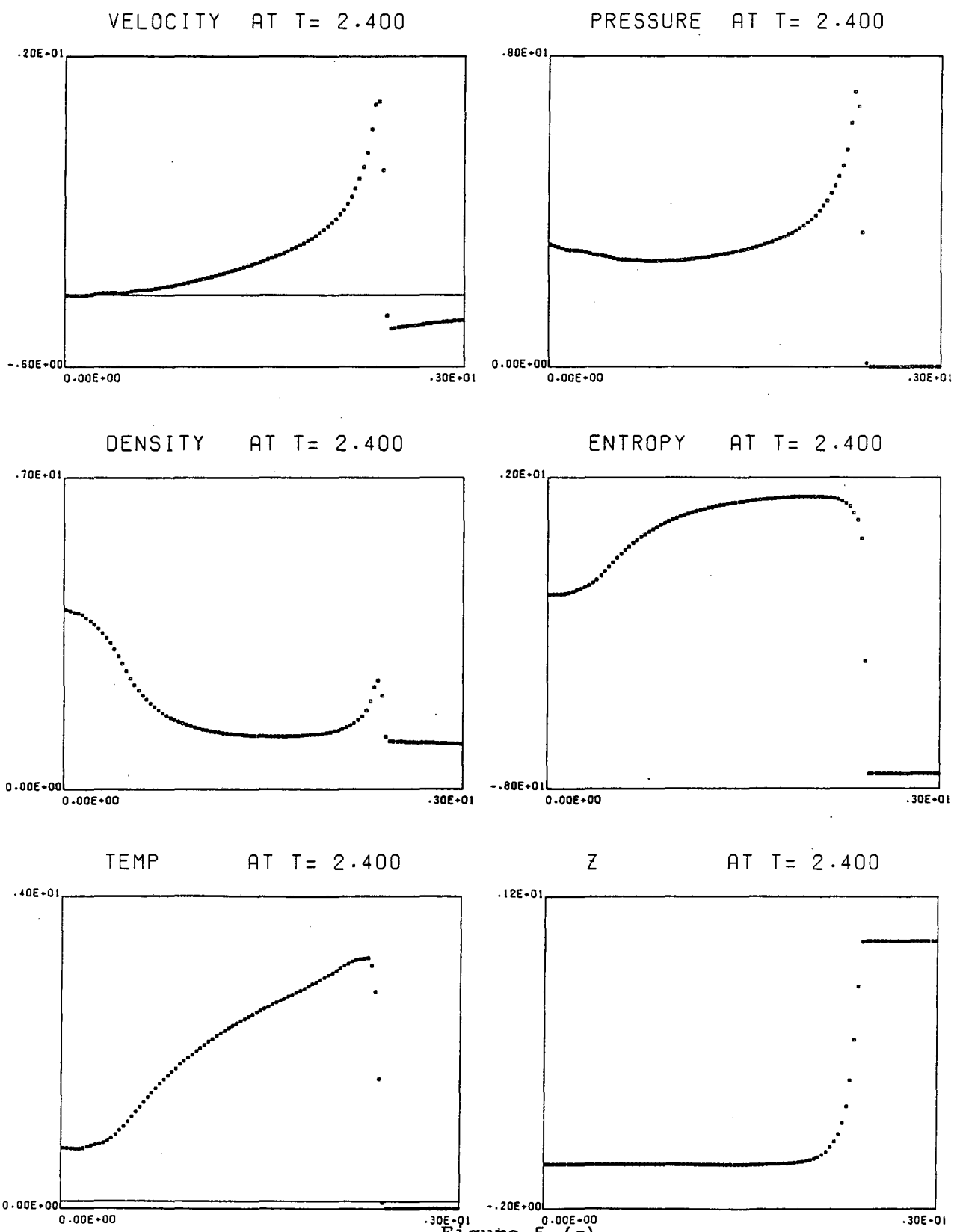

Figure 5 (c)

LAWRENCE BERKELEY LABORATORY
TECHNICAL INFORMATION DEPARTMENT
UNIVERSITY OF CALIFORNIA
BERKELEY, CALIFORNIA 94720